

# Recent progress on multiscale modeling of electrochemistry

Xiao-Hui Yang<sup>1</sup>  | Yong-Bin Zhuang<sup>1</sup>  | Jia-Xin Zhu<sup>1</sup>  | Jia-Bo Le<sup>2</sup> | Jun Cheng<sup>1</sup> 

<sup>1</sup>State Key Laboratory of Physical Chemistry of Solid Surfaces, iChEM, College of Chemistry and Chemical Engineering, Xiamen University, Xiamen, China

<sup>2</sup>Ningbo Institute of Materials Technology and Engineering, Chinese Academy of Sciences, Ningbo, China

## Correspondence

Jun Cheng, State Key Laboratory of Physical Chemistry of Solid Surfaces, iChEM, College of Chemistry and Chemical Engineering, Xiamen University, Xiamen 361005, China.  
 Email: chengjun@xmu.edu.cn

## Funding information

National Natural Science Foundation of China, Grant/Award Numbers:  
 21861132015, 21991150, 21991151,  
 22021001, 91745103

Edited by: Jinlong Yang, Associate Editor

## Abstract

Computational electrochemistry, an important branch of electrochemistry, has shown its advantages in studying electrode/electrolyte interfaces, such as the structures of electric double layers. However, modeling electrochemical systems is still a challenge, especially in interface electrochemistry, because not only solvation effects and ion distribution in electrolyte solutions should be considered, but also the treatment of the electrode potential and the response of electrolytes to applied potentials. Here, we review the latest development in the field of computational electrochemistry. We first introduce various energy models used in simulating electrolytes and electrodes at multiple scales. Then, to better explain and compare between different methods, we discuss the calculation methods of solution electrochemistry and interface electrochemistry in separate. At last, we introduce the methods to electrify the interfaces in various multiscale models. This review aims to help understand various levels of methods in simulations of different scenarios in electrochemistry, and summarizes a set of schemes covering multiple scales.

This article is categorized under:

Electronic Structure Theory > Combined QM/MM Methods

Molecular and Statistical Mechanics > Molecular Dynamics and Monte-Carlo Methods

Electronic Structure Theory > Density Functional Theory

## KEY WORDS

ab initio molecular dynamics, electric double layer, electrified interfaces, electrode potential, multiscale modelling

## 1 | INTRODUCTION

Electrochemistry is a broad research area that concerns various spatial scales ranging from atomic scale involving reaction mechanisms to macroscale focusing on industrial applications. Considering the wide range of scales, scale-dependent protocols should be employed in both experiment and computation for a trade-off between accuracy and efficiency. For example, *in situ* vibrational spectroscopy and ab initio molecular dynamics (AIMD) can be used to investigate the electrochemical reactions at the atomic scale.<sup>1</sup> By contrast, the researchers who concern the scientific problems at the macro scale might use other measurements (e.g., impedance spectroscopy) or numerical methods to study the performance of electrochemical devices.<sup>2</sup> Moreover, it is very common that one has to deal with problems of multiple scales in nature. Taking CO<sub>2</sub> electroreduction in alkaline polymer electrolytes as an example, one needs to consider

not only the proton transfer in the space charge layers of micrometer width in the polymer electrolytes, but also the microscopic coordination environment of  $\text{CO}^2$  at the electrocatalyst surfaces.<sup>3,4</sup> The examples mentioned above demonstrate the need for a set of methods covering multiple scales in studying electrochemistry, and we will focus on the multiscale modeling methods in this review.

Among various multiscale modeling methods, the atomistic models allow us to “see” the systems directly, and hence offer valuable insight into the detailed microscopic structures and physical properties at electrochemical interfaces. For example, using the all-atom simulation method such as ab initio molecular dynamics (AIMD), the water structure on the metal electrode can be directly observed under different electrode potentials.<sup>5</sup> The methods at the quantum mechanical (QM) level, however, suffer from high computational cost. As a result, such methods can only handle usually up to 1000 atoms with the current computing power, which significantly limits their applications to simulate complex systems. For systems of large sizes, calculation at the classical molecular mechanical (MM) level is a better option if the electronic structure information is less of a concern. For instance, solvation free energies of many ions and molecules can be accurately obtained in the MM simulations without describing electronic structures.<sup>6</sup> Furthermore, the interfacial structures and capacitances of large-size systems can also be investigated in MM simulations if a non-active electrode is employed, such as carbon electrode/room temperature ionic liquids (RTILs) interfaces in electric double layer capacitors.<sup>7</sup> However, suppose one wants to model even larger systems, such as polymer electrolytes in proton exchange membrane fuel cell (PEMFC) and alkaline polymer electrolyte fuel cell (APEFC). In that case, it may be even challenging for the MM models. The size problem could be alleviated by using the coarse-grained (CG) models, which merge a set of atoms into some virtual entities having certain shapes and interactions among each other.<sup>8</sup> The CG models still involve discrete particles. If this level of structural information is not of concern, it can be further reduced to continuum models, which only include the environment (i.e., implicit solvation) effects to the solutes/electrodes. The continuum models are suitable for describing the solvation environment, especially in homogeneous solutions. Extensive studies on the calculation of solvation free energies using implicit solvation models have been reported.<sup>6,9–15</sup> By using thermodynamic cycles, fundamental quantities such as redox potentials and acidity constants can also be obtained.<sup>16–20</sup>

This review aims to help readers focus on a full picture of simulation methods currently available in electrochemical simulations. To this end, the key features of the simulation approaches applicable to solution electrochemistry and interface electrochemistry are summarized in the four sections of this review. In the next section, the energy models used in electrochemical simulations are introduced, which directly determine the model size and time scale of the simulation. By applying these energy models in solution electrochemistry and interface electrochemistry, a variety of modeling methods have been developed in recent years. The characteristics and applications of these methods are introduced in Sections 3 and 4, respectively. In Section 5, the methods and models to electrify the interfaces are discussed. Finally, the review ends with some conclusion and outlooks.

## 2 | BRIEF INTRODUCTION OF ENERGY MODELS IN ELECTROCHEMICAL SIMULATIONS

In view of the intrinsic multiscale nature of electrochemical processes, it is impractical to use only one level of energy model in modeling electrochemical systems. Energy models are basic elements in multiscale modeling. The choice of these basic elements depends on the specific scientific problems of interest. In this section, we give a brief overview of the various energy models used in electrochemical simulations, the key features of these models, and the scopes to which they can be applied (Figure 1).

The fundamental microscopic description of electrochemical simulations is the all-atom (AA) models. In this models, all the chemical sites are explicitly introduced into the simulations, providing an atomic-level representation of the system. In general, the AA model can be treated at the QM or MM level (Figure 1(a)).

In QM energy models, both solutes and solvents are treated at the level of electronic structure theory where energies and forces are calculated from first principles (e.g., density functional theory [DFT]). Together with the information of electronic structure, QM energy models are able to simulate electrochemical reactions, such as  $\text{CO}^2$  electroreduction.<sup>19,22,23</sup> Computational accuracy is largely determined by the density functionals used. For example, the generalized gradient approximation (GGA) functionals often give poor predictions of electronic energies, which can be significantly improved by hybrid functionals at the expense of much increased computational cost. Cheaper empirical energy models, i.e. density functional tight-bonding (DFTB) models, is developed through parameterizing model

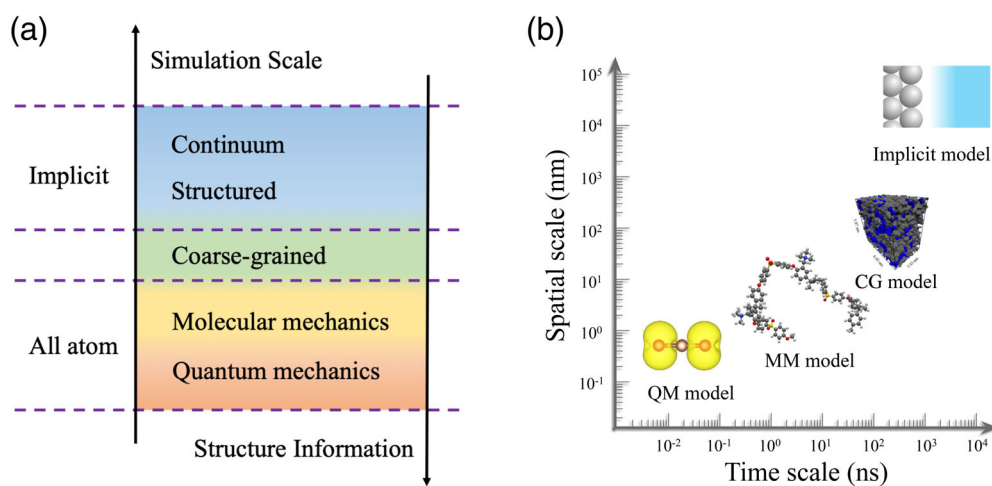


**FIGURE 1** Energy models used in simulations of electrochemical systems. (a) Schematic diagram of the structural information and model scales for these energy models. (b) Comparison of time and spatial scale among various energy models. (Reprinted with permission from Ref. 21)

Hamiltonians to give approximate electronic structures.<sup>24,25</sup> Although DFTB models are generally less accurate than the QM calculation, due to much reduced computational cost they have been successfully implemented in simulating complex solutions consisting of bulky solutes, such as RTILs.<sup>26</sup>

In MM models, atoms are represented by point charges, and their interactions are described by parameterized force fields accounting for bonding, dispersion and electrostatic forces.<sup>27</sup> In particular, chemical bonds, as predefined in a connectivity list, are modeled as harmonic springs omitting their quantum mechanical nature. Although several orders of magnitude cheaper than typical DFT calculation (Figure 1(b)), the obvious shortcoming of the MM models is that they cannot properly describe bond breaking and electron transfer processes. Nevertheless, MM energy models are computationally cheap, and are able to handle very large systems such as macromolecules and RTILs. With elaborated force field parameters fitting against accurate QM calculation or experiment, they can achieve similar accuracy to QM energy models in some aspects, for example, electrolyte structures.<sup>28</sup>

In usual MM models, the charges of atoms are fixed in the calculation, thus completely omitting possible electronic polarization in the process under study. To tackle this problem, the core–shell model is developed, which represents an atom with a positively charged core and a negatively charged massless shell, linked by a harmonic spring. The core and shell can move in the opposite direction in the presence of electrostatic interactions, and thus the polarization effect can be introduced by the net dipole of the core–shell structure.<sup>29</sup> In the application to gold electrodes, the core–shell model successfully reproduced classical image charge potential of adsorbed ions.<sup>30</sup> However, the linking between the core and shell limits its flexibility of describing electric polarization in the presence of external electric fields. In contrast, the Siepmann–Sprik potential model<sup>31</sup> describes the charge of each atom by Gaussian charge distribution, the magnitude of which can be adjusted according to a variational procedure to maintain constant electrostatic potential during calculation. Variability of the atom charges can better account for polarization effects of electrodes than the core–shell model\*. The Siepmann–Sprik potential model has thus been successfully applied to interface modeling of metal and carbon electrodes.<sup>32</sup>

To address the inability of describing bond breaking in the normal MM models, reactive force field (ReaxFF) models determine the bond connectivity on-the-fly according to the interatomic distances, which are assumed to directly relate to bond orders between pairs of atoms. A ReaxFF model has been developed to study dissociation of carbon–carbon bonds in hydrocarbons.<sup>33</sup> Bond breaking can be also described by empirical valence bond (EVB) models<sup>34,35</sup> and their extension, multistate EVB (MS-EVB).<sup>36–38</sup> In EVB models, the diabatic state of reactant (r) and product (p) are used to parameterize a model Hamiltonian involving a  $2 \times 2$  matrix of  $H_{rr}$ ,  $H_{pp}$  and 2 off-diagonal  $H_{rp}$ . To describe bond breaking, the adiabatic ground state potential energy is calculated by diagonalizing the matrix.

If atomic details are irrelevant to the problem of interest, it might be possible to replace the AA models with coarse-grained models in order to tackle larger size systems with lower computational cost (Figure 1(b)).<sup>39</sup> The CG models

improve the computational efficiency by reducing the number of degrees of freedom. For example, in order to describe polymer electrolytes, structures and dynamics of polymer chains are largely irrelevant to local monomer structures or high-frequency motions of individual atoms (e.g., water O–H vibrations),<sup>8,40</sup> and hence the degrees of freedom in polymer electrolytes can be reduced by grouping atoms in a monomer or a group of water molecules together into a single CG bead. By this means, both the time scale and spatial scale of CG simulations can be greatly increased compared with the MM energy model.

As for implicit models, the number of degrees of freedom is further reduced and only thermodynamically averaged properties are retained to describe solvent environments. In general, the implicit energy models can be classified into two types, that is, the continuum model<sup>41</sup> and the structured implicit model (Figure 1(a)).<sup>42,43</sup> The continuum model describes the solvation environment with the macroscopic dielectric constant which is approximated from the densities and charge distribution of solvent atoms. In comparison, the structured implicit model treats the distribution of solvent atoms as an independent variable, then optimizes it based on their intermolecular interactions (e.g., pair potentials).<sup>44</sup> Details of these two models will be introduced in the following section.

### 3 | SOLUTION ELECTROCHEMISTRY

The main challenge in the electrolyte modeling is how to describe the solvation environment of solutes adequately. In general, solutes are described explicitly by QM or MM energy models, and implicit or explicit models can describe the solvation environment. In implicit solvation models, only the thermodynamically averaged environment is described, often used for calculation of solvation free energies. In comparison, the explicit solvation models can offer more detailed information, such as hydrogen bonding structures in electrolyte solution. In this section, we introduce different solvation models for solution electrochemistry, and evaluate their accuracy in calculating solvation free energies and other thermodynamic quantities such as redox potentials.

#### 3.1 | Implicit solvation models

##### 3.1.1 | Continuum solvation models

Continuum models have been used as description for solvation of QM species for several decades,<sup>10,45–53</sup> and great efforts have been dedicated by pioneers to development and application of a variety of continuum models including the widely used solvation models (the SMx family)<sup>54</sup> polarizable continuum (PCM) model<sup>55</sup> and Conductor-like Screening Model (COSMO model).<sup>52</sup> Fattebert and Gygi<sup>56</sup> developed a continuum solvation model for first-principles molecular dynamics simulations, which was later extended by Marzari et al.<sup>12,57</sup> to include the contributions from cavitation and dispersion. Nowadays, the practice of the continuum solvation model is to first create a cavity around the solute, and then determine the dielectric constant as well as the charge distribution in the continuum solution. Therefore, challenges here in continuum models are how to determine the size of cavity surrounding the solute, and how to describe the solution's response to the solute inside the cavity.

The approaches to determine the cavity size in the continuum solvation models can be categorized into two groups, namely, the empirical atomic radii method and isodensity method. In the empirical atomic radii method, the cavity size depends on the empirical atomic radii (van der Waals radii is often used) of each atom of the solute molecule.<sup>58,59</sup> However, solute molecules usually have irregular shapes. To prevent the solvent response from being distributed in the small gaps between solute atoms, a popular method is to define a solvent molecular cavity with a smooth surface. The method first needs to estimate the surface that enclosing the volume in which the center of solvent molecules cannot enter. Then, shrink the SAS by a certain distance, which equals the radius of the solvent molecule. This newly formed smaller surface is called the solvent excluded surface (SES). At last, the location of the solvent response is determined.<sup>47,59</sup> The advantage of this atomic radii based method is that the cavity size can be tuned to obtain accurate results in a specific solvation simulation. The other, isodensity method correlates the cavity size to the electron density of the solute.<sup>56</sup> In this way, the cavity size can be determined based on the electron density of QM regions. Once the cavity size and surface are determined, the transition of the dielectric function from solute region to continuum solvent model is usually described by a smoothing function. The use of this smoothing function is to improve the numerical stability of computation near the QM/continuum boundary. Although the implementation of the smoothing function

varies with models, different smoothing functions generally give similar results when simulating the same systems.<sup>12,60</sup> In practice, discontinuities and singularities at the solute/solvent interface also can be repaired using the continuous surface charge (CSC) approach. This approach first expands the apparent surface charge that builds up at the solute/solvent interface in terms of spherical Gaussian functions located at each surface element in which the cavity surface is discretized. Then the discontinuities in the surface derivatives are removed by effectively smoothing the regions where the spheres intersect.<sup>61</sup>

After parameterizing the cavity size, we need to evaluate the solution's response to the solute. This response includes all interactions between the solute and the continuum model, which can be divided into two parts, namely, the electrostatic part and the non-electrostatic part. The electrostatic interactions of solvent molecules are described by the solvent dielectric constant. The other part is rather complicated because it deals with the interactions near the cavity interface. Generally, the contributions from the non-electrostatic interactions consist of four parts, that is, the formation energy of the cavity, the contribution due to thermal motion of the solute, the dispersion and repulsion interaction between the solute and the continuum model. Once the solute surface area and cavity volume are determined, the solvation free energy can be readily calculated. The electrostatic part can be directly obtained from the energy difference between the solute in the solution and the gas phase. The term due to thermal motion of the solute in solution can also differ from that in gas phase, and the difference can be estimated from approximated rotational and vibrational partitions functions of the solute. The formation energy of the cavity is estimated by the product of the experimental surface tension of the solvent and the surface area of the solute cavity. The last two terms, that is, the dispersion and repulsion energies, are usually derived from empirical formulas.<sup>12,60</sup> We recommend references<sup>46,48</sup> for detailed descriptions of the implicit solvation models.

Continuum solvation models such as SMx family, COSMO, and PCM can compute accurate solvation free energies thanks to sophisticated parameterization procedures and flexibility granted by a number of empirical parameters.<sup>62–69</sup> The solvation model density (SMD, one of SMx family) was used to represent the solvation effect in Dutra et al.'s<sup>63</sup> work studying the method of pK<sub>a</sub> calculation. The COSMO can reproduce comparable solvation effects with SMD, and was employed in Bamford et al.'s<sup>69</sup> work to determine the reaction pathway of B<sup>2</sup>(*o*-tolyl)<sup>4</sup> and boranes in computation. Tomaník et al.<sup>67</sup> compared the performance of both SMD and PCM solvation models in their new proposed method for the cluster-continuum calculation of solvation free energies. The mean absolute error (MAE) in these models are less than 1 kcal/mol for neutral solutes and about 4 kcal/mol MAE for charged solutes. These models have been already implemented in various quantum chemistry codes,<sup>†</sup> and recent models such as the self-consistent continuum model (SCCS),<sup>12</sup> have been devised to minimize the number of empirical parameters. With the continuous improvement by follow-up works,<sup>58,60,70,71</sup> the SCCS model relies on a much-reduced number of parameters, and is able to obtain solvation energies with a reasonable MAE of about 1.2, 2.27, and 5.54 kcal/mol for neutral solutes, cations and anions, respectively.<sup>60</sup> Since considerable errors in continuum models come from the omission of self-dissociating species and strong hydrogen-bond-forming compounds, the inclusion of a few explicit solvent molecules around the solute has become a common practice to improve the accuracy of these difficult cases. However, if explicit solvent molecules were included, the configurations of the whole cluster (i.e., orientation and diffusion of explicit molecules) involve much more degrees of freedom. These extra degrees of freedom, as well as the treatment of explicit solvent molecules at the QM level, can significantly increase the computational cost.

### 3.1.2 | Structured implicit solvation models

A more sophisticated alternative to the continuum solvation model mentioned above is the structured (cavity-less) implicit solvation model, which directly treats the solvent distribution as an independent variable and optimizes it based on the interaction of the solvent with the solute.<sup>42,72,73</sup> Therefore, more detailed structure information such as solvation shell structures and ion distribution can be obtained. Two types of structured implicit solvation models have been developed, that is, the reference interaction site method (RISM)<sup>74,75</sup> and the classical density-functional theory (classical-DFT).<sup>43</sup> The RISM model establishes integral equations on the solvent density based on correlation functions and interaction potentials of the solvent, and the interactions with QM solute also use interaction potentials (such as pair potentials in classical force fields).<sup>73,76</sup> In contrast, the classical-DFT directly approximates the free energies as functionals of the density of solvent molecules, and its interactions with QM solute can be solved by the joint density-functional theory (JDFT). The JDFT proposes to join the electron density functional for the solute with classical-DFT for solvents into a single variational principle for the free energy of the combined system.<sup>77–79</sup> Otani

et al.<sup>73</sup> reformulated the three-dimensional RISM (3D-RISM) method<sup>80,81</sup> and calculated the hydration free energy of water and formaldehyde with errors of 2 and 4 kcal/mol compared with experiment, respectively. The JDFT model developed by Arias et al.,<sup>79</sup> involving a single solvent-independent parameter plus a single solvent-dependent parameter, can compute the solvation free energies of organic molecules in water, chloroform, and carbon tetrachloride with small error of 1.1, 0.6, and 0.5 kcal/mol, respectively. Based on the reported calculation of solvation free energies,<sup>79</sup> the structured implicit models, with smaller number of empirical parameters, show similar level of accuracy to the conventional continuum model (e.g., PCM model). Thus, the structured implicit solvation methods are expected to have better transferability to complex systems.

### 3.2 | Explicit solvation models

Turning to explicit solvation models, two points should be noted beforehand. First, unlike the implicit solvation model involving an infinitely large solution environment, only a small number of explicit solvent molecules centered on the solutes under open boundary conditions, are usually insufficient to represent the actual solution environment in the condensed phase. In this case, it is common to apply the full periodic boundary conditions (PBC). A unit cell replicates periodically such that sufficient solvent molecules are included to reproduce the solution environment in the simulation model. Second, solvent properties such as polarization and diffusion are explicitly described in the explicit solvation models, giving rise to a large number of degrees of freedom in the simulated systems. Therefore, statistical sampling is required to collect sufficient configurations to ensure the converge of thermodynamic properties of interest, and computational techniques like molecular dynamics (MD) and Monte Carlo (MC) are often used to perform sampling of configurational space.<sup>19,82</sup> Since explicit solvent models can compute not only the solvation free energies, but also electrolyte structures. In this section, we first briefly introduce free energy calculation with sampling methods using explicit energy models, and then discuss various multiscale schemes, for example, QM/MM model, for free energy calculation.

#### 3.2.1 | Free energy calculation by explicit models

If the explicit solvation models are represented in purely the MM or QM level, solvation free energies can be obtained by using various free energy calculation schemes, such as thermodynamic integration (TI) and free energy perturbation (FEP).<sup>9,83–86</sup> The FEP/TI scheme is commonly used for calculating free energy differences between the initial and final state with a coupling parameter  $\eta$  (key equations are summarized in the middle panel in Figure 2). A fictitious hybrid energy state can be defined as  $H_\eta = (1 - \eta)H_0 + \eta H_1$ , with  $H_1$  and  $H_0$  the energy of the initial and final states, respectively. The derivative of  $H_\eta$  with respect to the coupling parameter corresponds to the energy difference between the final and initial states at a fixed configuration ( $\partial H_\eta / \partial \eta = \Delta E = H_1 - H_0$ ).  $\Delta E$  is the vertical energy gap and can be obtained from the electronic structure calculation as a total energy difference.  $\Delta E$  is then averaged over molecular dynamics (MD) runs for a sequence of values of  $\eta$ . Integration of the thermal average  $\langle \Delta E \rangle_\eta$  along the thermodynamic path ( $\eta$  from 0 to 1) converts vertical into adiabatic free energies  $\Delta A$ . In solvation free energy calculations, initial and final states are computed by reversibly inserting the solutes in simulations. The same method can be used to calculate adiabatic ionization energies (AIP) and adiabatic deprotonation energies (ADP), as indicated by blue arrows in upper left panel of Figure 2, by replacing solutes in both initial and final state as  $X^-/X$  and  $HX/X^-$ , respectively.

Unfortunately, the calculated ionization free energy ( $\Delta_{\text{ox}}A_{X^-}$ ) and deprotonation free energy ( $\Delta_{\text{dp}}A_{XH}$ ) are not yet equal to the AIP and ADP that we want to calculate, owing to the fact that the reference of the electrostatic potential is uncertain in the standard Ewald summation under PBC and spurious interactions of particles in the cell and their periodic images and neutralizing background.<sup>6,87</sup> The energy of an anion  $X^-$  under PBC is shifted by an unknown energy  $e_0V_0$ , as shown by an orange arrow in the bottom left panel of Figure 2. Consequently, the values of  $\Delta_{\text{ox}}A_{X^-}$  and  $\Delta_{\text{dp}}A_{XH}$  alone are yet to bear any physical meanings. On the other hand, the calculated deprotonation free energy of aqueous hydronium ( $\Delta_{\text{dp}}A_{H_3O^+}$ ) has the same shift  $e_0V_0$ . If the aqueous hydronium is taken as reference ion, a meaningful value of acidity constant for  $HX$  in aqueous solution and redox potential for  $X^-$  with respect to the standard

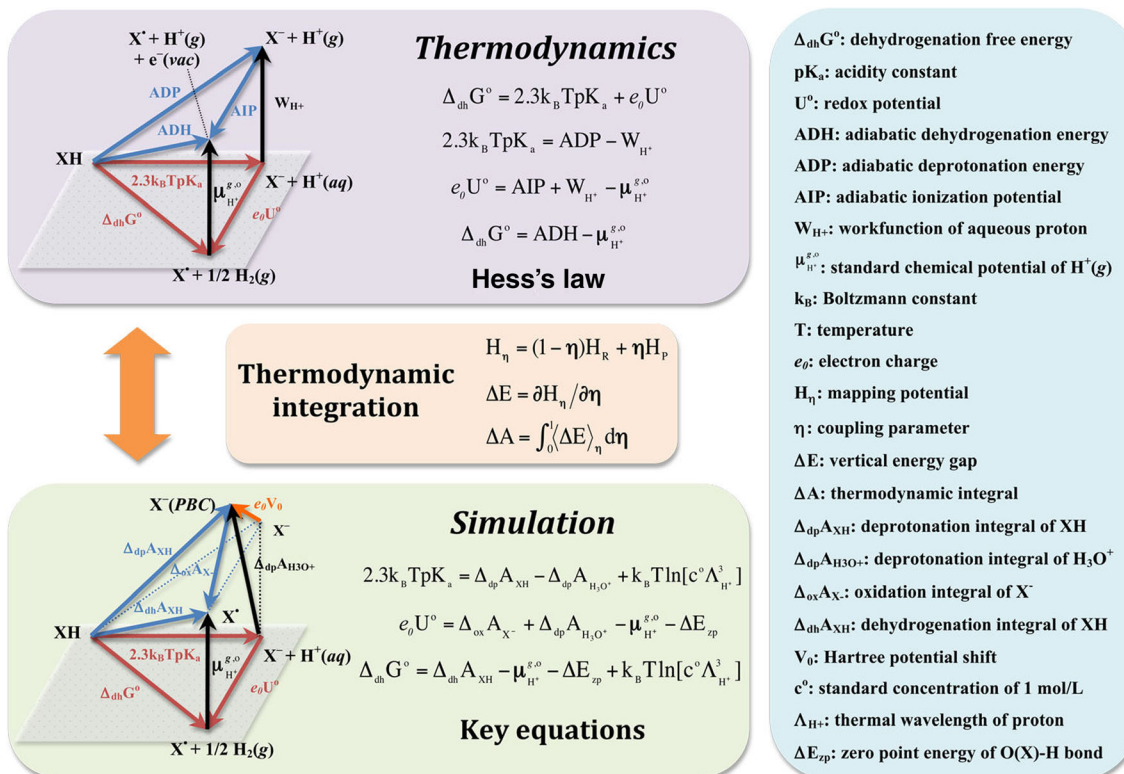


**FIGURE 2** Schematic representation of the ab initio molecular dynamics based method for computing redox potentials and acidity constants. (Reprinted with permission from Ref. 91)

hydrogen electrode (SHE) can be obtained, as indicated by the red arrows in the bottom left panel of Figure 2. Using the hydronium like structure as an approximated model for the solvated proton has been discussed and justified in appendix of Ref. (88). The acidity constant in aqueous solution can be estimated by subtracting  $\Delta_{dp}A_{H_3O^+}$  from  $\Delta_{dp}A_{XH}$ . Similarly, the redox potential versus SHE can be obtained by adding  $\Delta_{dp}A_{H_3O^+}$  to  $\Delta_{ox}A_{X^-}$ .

As a feasible scheme in AIMD simulations, this method has been successfully utilized to calculate acidity constants and redox potentials for a number of small inorganic and organic molecules.<sup>16,19,89–92</sup> The computed results can be directly compared with the experimental values with an error of about 1–2 pKa units for acidity constants but a much larger error (ca., 0.5 V) in redox potential calculation using the GGA functional.<sup>91</sup> Poor performance in redox potential calculation, in fact, is due to the well-known delocalization error in DFT approximations, and this error can be reduced to 0.2 V if hybrid functional, for example, HSE06, is employed.<sup>91,93</sup> Although the AIMD based method can be readily used for any solution in principle, it incurs a substantial computational cost, significantly limiting its application to complex solutions having multiple components or sluggish dynamics.

### 3.2.2 | Quantum mechanical/molecular mechanical solvation models

The QM/MM model can tackle a larger spatial scale and time scale compared with the QM model, and thus is able to alleviate finite size effects under PBC and extend the scope of application in simulating solution environments such RTILs. Generally, solvent molecules in the vicinity of the solute are treated at the QM level, and the MM energy model represents the remaining part to reduce the computational cost.<sup>94</sup> The key to the QM/MM model is how to treat the coupling between the QM and MM regions. Generally, this coupling consists of two parts, that is, the potential coupling and the dynamic coupling.<sup>95</sup> The potential coupling refers to the interactions between QM solutes and MM molecules, and is often handled by pair potentials. Pair potentials can be divided into two parts, non-electrostatic interactions and electrostatic interactions. The non-electrostatic part of pair potentials (i.e., van der Waal interaction) is usually described by empirical formulas such as Lennard Jones potentials. In term of the electrostatic interactions, the

commonly used protocol is the electrostatic embedding, which couples interactions between the electron density and nuclear charges in QM region and the point charges in the MM region.<sup>96–101</sup> Calculation of electrostatic energies in QM/MM simulations is a time-consuming process, and needs to treat the electrostatic interactions in the system which includes classical point charges in the MM region, nuclei charges and electron densities in the QM region. To improve the computational efficiency of this step, point charges based on electrostatic potentials can be employed to represent QM solutes, although this method overestimates electrostatic interactions at short-range interactions.<sup>99</sup> An approach to avoid this problem is to use real space grids to represent electrostatic potentials for both QM and MM region.<sup>96,99,102</sup> Figure 3(a) is an example of grid-based electrostatic embedding approach developed by Yamamoto et al.<sup>99</sup> They pre-calculated the electrostatic potentials on the grid points in the QM region, and interpolated them in MD simulations. In this way, efficient sampling of MM molecules in the presence of QM molecules can be achieved. Kim et al.<sup>102</sup> later extended this grid-based electrostatic embedding method by including the geometric and electronic responses of solutes to solvation effects in a self-consistent manner. This method, call as density functional theory in classical explicit solvents (DFT-CES), can be further coupled with free energy calculation based on the two-phase thermodynamic (2PT) model to calculate solvation free energies.

The other coupling between the QM and MM regions, that is, the dynamic coupling, needs to be considered when molecules in the QM or MM region have the probability of transferring into the other's region. This coupling is crucial in QM/MM calculation of the liquid phase in which molecules have high diffusivity. A simple and straightforward approach to address this issue is to constraint QM and MM regions by applying restraining potentials, to prevent QM and MM molecules from escaping their original region.<sup>103,104</sup> Roux et al.<sup>103</sup> developed a QM/MM model with

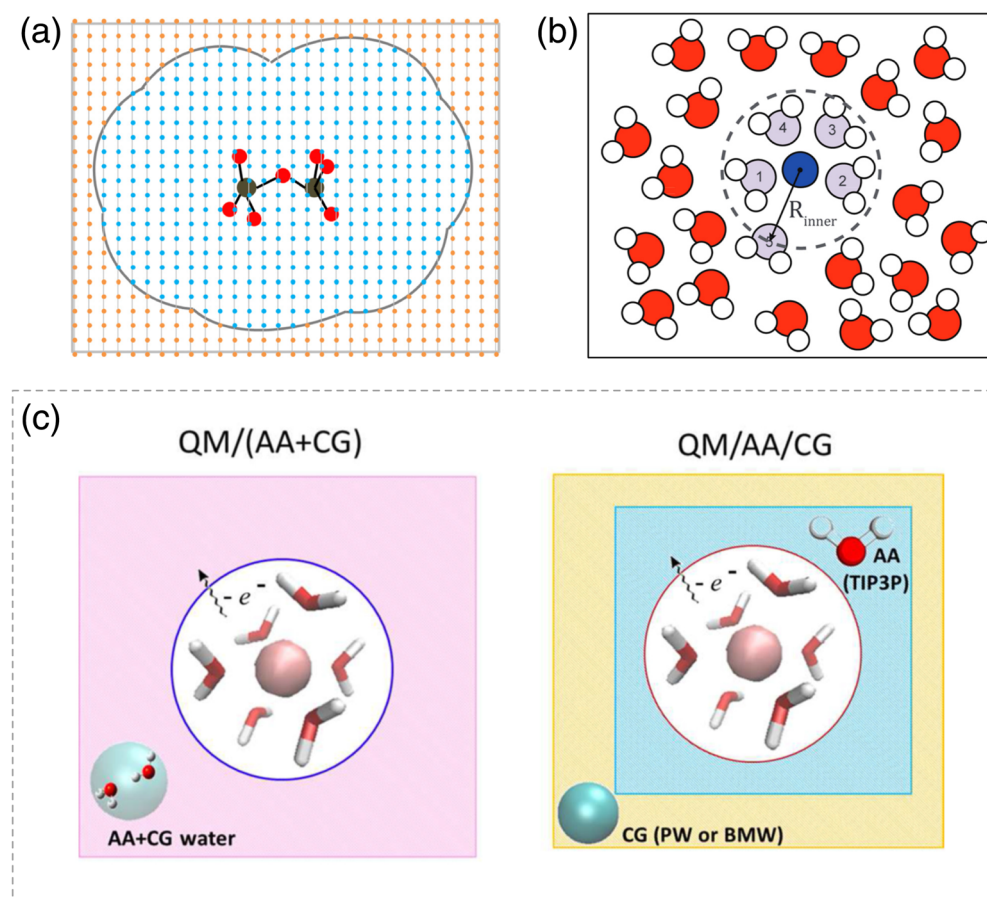


**FIGURE 3** (a) Schematic view of grid-based treatment of electrostatic potentials. Only electrostatic potentials on the grid points are employed in the QM/MM electrostatic embedding calculations, where blue and orange represent the QM and MM regions, respectively. (Reprinted with permission from Ref. 99). (b) Schematic view of the QM/MM model with restraining potentials (dashed circle). Molecules inside and outside the circle are QM molecules and MM molecules, respectively. The  $R_{inner}$  is the radius of the dashed circle. (Reprinted with permission from Ref. 103). (c) Schematic representations of QM/(AA+CG) (left) and QM/AA/CG (right) models under PBC without the Ewald summation technique. (Reprinted with permission from Ref. 20)

restraining potentials (Figure 3(b)) to compute the solvation structures of  $\text{Na}^+$  and  $\text{K}^+$  in water, and obtained their coordination numbers. In addition to restraining potentials, the adaptive QM/MM approach can be employed, which allows the solvent molecules to be reclassified on-the-fly as QM or MM during the MD simulations. In this way, solvent molecules entering into the active region can always be defined as the QM molecules. Common adaptive QM/MM approaches also include a buffer zone to gradually transform the molecular description between the QM and MM model.<sup>95</sup> Although various adaptive QM/MM methods have been verified by comparing solvation structures with full QM or conventional QM/MM simulations,<sup>28,105</sup> adaptive methods are unable to achieve energy conservation yet. Discussions about the adaptive methods can be found in reference.<sup>95,106</sup>

Apart from explicit models developed under PBC, Yang et al.<sup>107,108</sup> proposed an approach under open boundary conditions to calculate redox potentials of the aqueous ruthenium and iron complexes in aqueous solutions. The implementation of open boundary conditions, achieved by employing a long cut-off distance of pair potentials, can avoid the technical complications in computing charged systems under PBC. Based on their previous development, they further developed a new multiscale scheme recently, that is, the QM/(AA + CG) model, which combines QM, MM, and CG, three energy models.<sup>20</sup> In this scheme, the redox center is represented by the QM energy model, and the environment water molecules are represented by an integrated MM model and CG model (adaptive AA + CG model). The interactions between atoms at a short distance are described at an explicit AA level, while the interactions at a long distance are modeled at a CG level. Therefore, the QM/(AA + CG) model (presented in the Figure 3(c), left) can effectively describe long-range electrostatic interactions compare to QM/MM models. Yang et al. also compared their QM/(AA + CG) model with another multiscale scheme, that is, the QM/AA/CG model (Figure 3(c), right) including also three energy models of QM, MM, and CG. In the QM/AA/CG model, environment water molecules close to the QM redox center are described by MM models, while water molecules far away from the QM region are grouped together and represented by a sophisticated CG model, which should be distinguished from the adaptive AA + CG model used in the QM/(AA + CG) model. The calculated redox potentials of the aqueous ruthenium and iron complexes indicate that the QM/AA/CG model is less accurate than the QM/(AA + CG) model, with the latter being in excellent agreement with experiment (error within 0.1 eV). The authors suggest that the errors in redox potentials computed with the QM/AA/CG model are due to the inaccuracy of the CG model in describing QM/MM electrostatic interactions.

### 3.2.3 | Other explicit models for electrochemical applications

One advantage of explicit models over continuum models is that they can provide structural and dynamic information of electrochemical systems, such as electrolyte structures<sup>109</sup> and ion diffusion.<sup>110</sup> With the current computing power, AIMD can normally simulate the structures of the systems on the order of 1000 atoms at a time scale of 10–100 ps. However, it is insufficient for many scenarios in electrochemistry which require simulations of a much larger spatial scale and longer time scale. Semi-empirical DFTB models are usually 1000 times faster than the standard DFT calculation, offering a good option for modeling larger-sized systems. For example, Perlitz et al.<sup>26</sup> compared the RTILs structures obtained from multiple DFTB models with the QM model, and suggested that the DFTB models are a promising method for future large-scale simulation. In addition, an elaborate parameterized MM energy model can also calculate very reasonable structural and dynamic results compared with AIMD. For example, the MS-EVB model<sup>111,38</sup> can even give better diffusion coefficients of  $\text{H}^+$  and  $\text{OH}^-$  ions in electrolytes than the DFT model at the GGA level.<sup>112</sup> Despite the promising progress, the MM models may not be effective in describing the folding behaviors of polymer electrolytes, and the CG models are proven to be a better choice for studies of polymer membranes.<sup>40,113</sup> Using a CG model, Zhuang et al.<sup>114</sup> studied the influences of the side chain length of alkaline polyelectrolytes and water content on the conductivity of the polyelectrolytes. If it is necessary to include the electronic structures in large systems, the embedding models, that is, QM/(AA + CG) or QM/AA/CG model in Figure 3(c), are feasible multiscale approaches.<sup>20</sup> Recently, Voth et al.<sup>115</sup> combined the ideas of QM/MM and CG modeling into a unified “QM/CG-MM” method, which describes the entire surrounding of the QM region by CG models.<sup>116,117</sup>

In summary, different solvation models have their special characteristics suitable for certain types of applications. From the QM, MM, to the CG models, scales of simulations increase significantly. However, this is based on reducing the number of degrees of freedom of solvents, which inevitably reduced the structural information contained in solvation models. QM models include adequate structural information at the atomic level compared with hybrid models (such as QM/MM and QM/(AA + CG)) or implicit models. For example, the QM model is often used for the cases where solvent molecules play a vital role, for example, strong hydrogen-bond interactions and charge transfers between the solute and solvent molecules. However, the computational cost limits the use of the QM model. It is required to

choose a suitable model according to the problems of interest, to balance the accuracy and efficiency of our computation. This is the scenario where we started to consider using cheaper models such as MM, CG models and hybrid models. Moreover, implicit solvation models can account for the solvation effects of most solutes in homogeneous solution with low computational cost. Thus, they are often employed in solvation energy calculations.

## 4 | INTERFACE ELECTROCHEMISTRY

Electric double layers (EDL) at the electrode/electrolyte interfaces are where electrochemical reactions occur and are of paramount importance in electrochemistry. However, microscopic understanding of the EDL is still lacking due to its complexity and difficulty to probe. Thanks to the development of computational methods, modeling has shown great potential in studying the interface of the electrode and the electrolyte in the past few years, and provided valuable insight into EDL structures and dielectric properties.<sup>5</sup> One of the key characteristics of EDL is its capacitance measuring the ratio of change in surface charge density to potential change. It can be obtained by voltammetry experiment, and thus can serve as a benchmark quantity for modeling methods. Replacing finite size solutes in the models described in the last section with two-dimensional infinite electrode surfaces, we turn to modeling of interface electrochemistry. In the following, we omit similar simulation details and focus on the performance of EDL modeling.

### 4.1 | Quantum mechanical/implicit interface models

Similar to the solution, the QM/continuum models for interfaces describe the electrodes and solvents by QM and continuum models, respectively. A vacuum gap, like the cavity in the continuum solvation models, is included between the electrode (QM) and the electrolyte (continuum), as shown in Figure 4(a). The vacuum thickness  $x_1$  shown in Figure 4(a) is usually determined by the isodensity method with smoothing functions used to smoothly transform dielectric

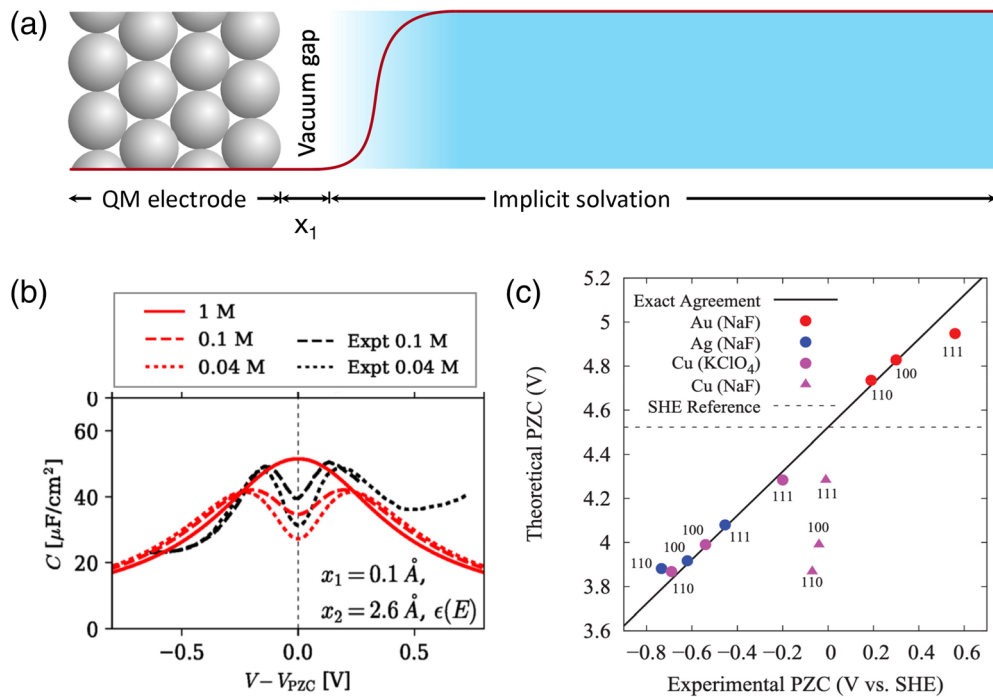


**FIGURE 4** (a) Schematic illustration of QM/continuum interface model. The electrode is represented by QM model, and the large blue region is the implicit electrolyte region. The red curve represents the variation of the dielectric constant from the QM electrode (i.e., 1) to the bulk of solution continuum (i.e., 78). (b) Comparison between computed and experimental capacitances of Ag(100) in aqueous solution. Toy models consist of non-linear solvent and electrolyte ions response with vacuum gap thickness  $x_1$  and extended distance  $x_2$  (i.e., distance between ionic radius  $r$  and vacuum thickness  $x_1$ , and  $x_2 = r - x_1$ ) to the surface. (Reprinted with permission from Ref. 59). (c) Comparison between potentials of zero charge computed by the JDTF surface model at the DFT-GGA level and experimental data<sup>122</sup>

constant from electrodes to continuum solutions (see the red curve in Figure 4(a)). Smoothing functions may take different forms in different models, but have the same purpose of improving numerical stability of calculation. In continuum interface models, the distribution of electrolyte ions is often described by the Poisson–Boltzmann (PB) model.<sup>56,118</sup> If the electrode is charged, ions in electrolytes gather around the charged electrodes. However, the PB model cannot properly describe this charge accumulation because the PB model lacks the description of the repulsion between ions. As a result, it overestimates ionic concentrations at the charged surface.<sup>119,120</sup> The Modified Poisson–Boltzmann (MPB) model<sup>121</sup> adds a “packing limit” on the ions to account for the finite size of the ions, in which a maximum ion concentration determined by the ionic radius  $r$ , is imposed to limit close packing of ions at the charged surface. Specifically adsorbed species often require quantum mechanical treatment, and thus should be included in the QM region. The charges in the continuum model described by the MPB can only accumulate in the outer Helmholtz layer. Thus, the distance (i.e., ionic radius  $r$ ) between ions and the surface is longer than that for solvent molecules. Using the proper ionic radius in the QM/continuum interface model, Sundararaman et al.<sup>59</sup> successfully predicted the capacitance curve in excellent agreement with experimental results (Figure 4(b)).

In addition to the continuum models mentioned above, solutions can also be described by structured solvation models, for example, the RISM and JDFT model. Treatment of interactions between electrodes and electrolyte in these structured interface models are very similar to those in the liquid phase simulations (Section 3.1.2). Figure 4(c) shows the potential of zero charge (PZC) of various single-crystal metal surfaces predicted by the JDFT method versus experimental values.<sup>72</sup> The linear correlation with unit slope between the theoretical and experimental data indicates that the JDFT model can reasonably predict the PZC of the metal surfaces. Recently, Wang et al.<sup>123</sup> employed the JDFT method to investigate the charging behavior of the Ag(111) electrode in NaF aqueous solutions.

## 4.2 | Explicit interface models

### 4.2.1 | Quantum mechanical or molecular mechanical interface models

AIMD is often used in calculation of interface electrochemistry, and the results can be used as benchmark for other models to verify their accuracy.<sup>124</sup> By using the AIMD interface model, Le et al.<sup>125</sup> successfully calculated the PZC of metal/water interface with an error of less than 0.1 eV. They further concluded that at the PZC condition, interface dipole potentials are determined by the charge redistribution from chemisorbed water to the metal electrodes (Figure 5(a)) while water orientation has a negligible contribution. Le et al.<sup>1</sup> then investigated the EDL of Au(111)/water interface (Figure 5(b)) and revealed the existence of three characteristic, potential-dependent water configurations (“parallel,” “one-H-down,” and “two-H-down” water) at the Au(111)/water interface. Recently, Le et al.<sup>5</sup> simulated the electrified Pt(111)/water interfaces and found that the coverage of chemisorbed water molecules increases when shifting the potential from negative to positive, which follows the Frumkin adsorption isotherm. The coverage change of chemisorbed water molecules can induce significant interface dipole potential change, and result in a negative capacitive response (Figure 5(c)). These works demonstrate the importance of electronic structure description of the interface in correctly treating electrode potential and dielectric response of interface water, which can only be accounted for in AIMD simulations.

Simulations at the interface can also use MM energy models.<sup>7,30–32</sup> As introduced in the Section 2, two commonly used methods to describe energy models of electrodes are the core–shell model and the Siepmann–Sprik potential. Recently, Henzi et al.<sup>30</sup> proposed a core–shell model for gold electrode. This core–shell model has good compatibility, as it only consists of a Lennard-Jones potential and a harmonically coupled pair of opposite charges for every metal atom. However, the charged shell in the core–shell model is tethered to the positively charged core and cannot move freely. Therefore, this core–shell model cannot reproduce internal charge distribution of metal electrodes in the presence of external electric fields.<sup>30</sup> To describe internal charge distribution in simulations, the Siepmann–Sprik potential can be used. This method constant potential electrodes that screen the field inside the bulk region of electrodes, and this method has been implemented in many interface simulations, for example, modeling electric double layer capacitors.<sup>7,31,32</sup>

### 4.2.2 | Quantum mechanical/molecular mechanical interface models

In QM/MM interface models, the regions for which the QM or MM model is used can be flexible, and depend on the topics of interest in interface electrochemistry. For example, Kim et al.<sup>4</sup> recently extended their DFT-CES model to

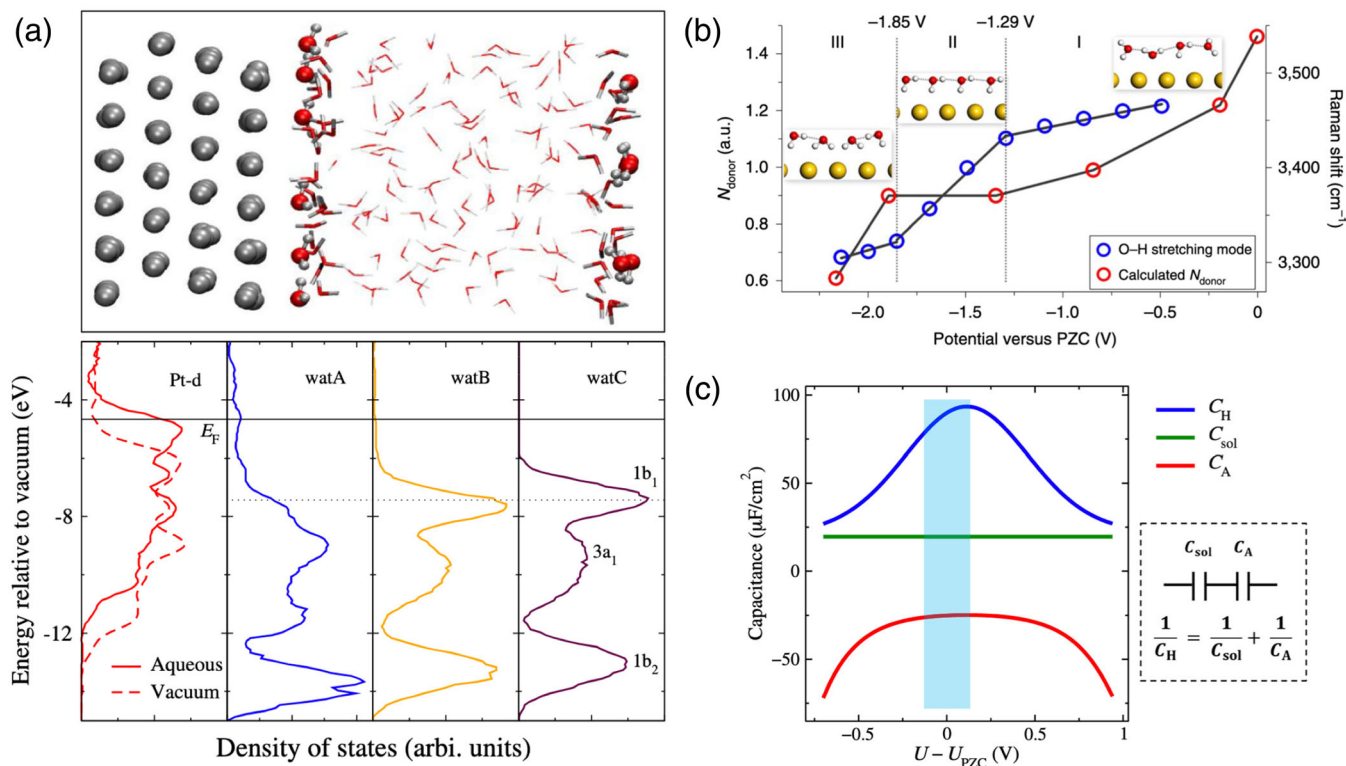


**FIGURE 5** (a) Snapshot of the Pt(111)/water interface model (top), and the projected density of states (PDOS) plots (bottom) of Pt and water molecules at the interface computed by the PBE functional. In this figure, water molecules adjacent to the Pt surface with the dipole pointing away from the surface is called watA. The PDOS of watA is lower than the Fermi level of the Pt electrode, which proves that there are a few water molecules close to the surface (i.e., watA) chemisorb on Pt. (Reprinted with permission from Ref. 125). (b) Potential-dependent evolution of the hydrogen-bond network of interface water. Insets are structure models of interface water in the corresponding potential regions. (Reprinted with permission from Ref. 1). (c) Capacitance model of the Helmholtz layer. Decomposition of differential Helmholtz capacitance  $C_H$  (blue) as a function of electrode potential  $U$  into two constituent components, i.e. the normal capacitance  $C_{\text{sol}}$  (green) of interface water and the capacitance  $C_A$  (red) due to chemisorbed water. The inset indicates that  $C_{\text{sol}}$  and  $C_A$  are connected in series. (Reprinted with permission from Ref. 5)

interface simulations between silver surface and water/EMIM-BF<sub>4</sub> mixture electrolytes (Figure 6(a)). In this DFT-CES interface model, the silver surface and water/EMIM-BF<sub>4</sub> mixture electrolytes are described by QM and MM energy models, respectively. This multiscale model can be used for the statistic sampling up to the nanosecond time scale, affording sufficient simulation time to equilibrate bulky ions like EMIM<sup>+</sup> and BF<sub>4</sub><sup>-</sup> in the electrolyte solution. To study chemisorption on metal surfaces, Hutter et al.<sup>126</sup> proposed an image charge augmented QM/MM (IC-QM/MM) method. This IC-QM/MM method combines a QM described nitrobenzene molecule and the Siepmann-Sprik potential described Pt(111) electrode, and hence can reproduce the electric response of the nitrobenzene charge density to the induced charges of the electrode (Figure 6(b)). All the above QM/MM schemes performed under PBC, while a non-PBC QM/MM method was developed by Stecher et al.<sup>101</sup> for a study of the water splitting reaction on rutile TiO<sub>2</sub>. This non-PBC QM/MM method avoids complexity under PBC due to charged defects in oxide electrodes. In this non-PBC QM/MM model, a final exterior shell of point charges is added at the outer boundary of the finite MM region to reproduce the full electrostatic potential of the surface inside the QM region (Figure 6(c)).

The importance of chemisorbed water at metal/water interfaces has been demonstrated by using AIMD simulations, which indicates the charge transfer between solutions and electrodes needs to be properly considered. Thus, AIMD should be the recommended method for modeling active interfaces where solvent molecules or other reactive species chemisorb on the electrode surfaces. Of course, the downside is its high computing cost significantly limiting the time scale and model size of the simulations. The QM/MM and QM/implicit model usually set the boundaries between the energy models right at the electrode-electrolyte interface, and thus are not suitable to account for the effect of charge redistribution at the interface. Recently, Marzari et al. proposed an interface model that includes a few layers of QM solvation molecules to describe the chemisorbed solvents at the interface.<sup>71,127</sup> However, how to determine the location of

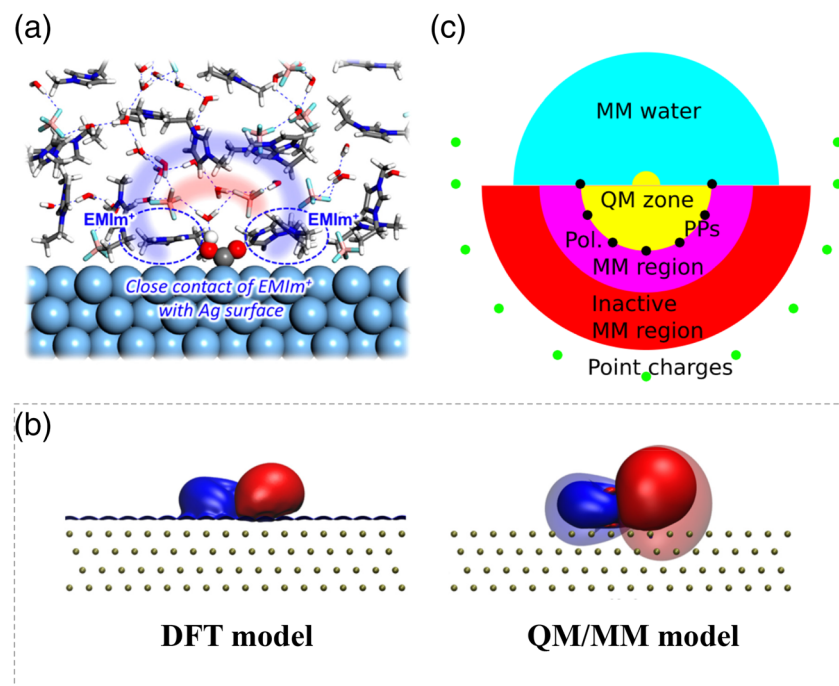


**FIGURE 6** (a) Side view of the QM/MM interface model including the water/EMIM-BF<sub>4</sub> mixture as the electrolyte on Ag(111) surface. (Reprinted with permission from Ref. 4). (b) Model of nitrobenzene on Au(111). Isosurface of the electrostatic potential obtained with full DFT (left) and QM/MM model (right). The transparent isosurface is from the conventional QM/MM model, and the solid isosurface is from the IC-QM/MM model. (Reprinted with permission from Ref. 126). (c) Schematic illustration of the electrostatic QM/MM cluster embedding model used for the TiO<sub>2</sub>/water interface. (Reprinted with permission from Ref. 101)

the boundary between explicit and implicit solvation model is still an open question, which also exists in QM/MM interface models. Specifically, the challenge is how to minimize the effect of solvation structures near the QM/implicit (or QM/MM) boundary on the EDL structures when varying electrode potential, and at the same time, keep explicit solvent molecules in the QM region as few as possible. If a large number of QM solvent molecules are included at the interface, the number of degrees of freedom will increase significantly, and the consequence is that statistical sampling becomes inevitable, leading to an increase in the computational cost.

## 5 | ELECTRIFYING INTERFACE MODELS

Modeling interface electrochemistry requires to maintain the electrode potential of a working electrode with respect to a reference electrode. Keeping the electrochemical potential of electrons under control, inevitably leads to fluctuation of the number of electrons in the working electrode. The method for constant electrode potential is simulating this electrode in grand canonical ensemble.<sup>128–133</sup> As an alternative, the variation of electrode potentials can also be achieved by varying the charges of electrode in a half-cell model in canonical ensemble. The other choice rather than a half-cell model is directly simulating a full-cell in canonical ensemble<sup>134,135</sup> since the number of electrons is conserved in the full-cell model. In this section, we summarize the methods for controlling electrode potentials in half-cell models (both canonical and grand canonical ensemble) and full-cell models.

### 5.1 | Half-cell models

In order to maintain constant chemical potentials, half-cell models in the grand canonical ensemble use an external electron reservoir to adjust the number of electrons in the system. This significantly differs from the standard DFT implementation in which ground state electron densities are obtained through optimization of Kohn-Sham (KS) orbitals in the self-consistent field (SCF) iterations with the total number of electrons fixed. Rather, one can resort

to the grand canonical DFT (GC-DFT) formalism in which the number of electrons are determined in the SCF loop to target at a specified electron chemical potential.<sup>128,131</sup> This GC-DFT optimization procedure, however, is usually very expensive and difficult to converge. One way to go around this problem is to use multiple standard fixed-number DFT calculations in an outer loop which is considered as converged until a trial number of electrons gives a pre-set electron chemical potential.<sup>136</sup> Another interesting approach developed by Otani et al.<sup>130</sup> enables AIMD simulations at constant electrode potential. In this scheme, the simulation system is connected with a fictitious potentiostat, analogous to the Nose–Hoover thermostat in constant temperature MD calculation. An appealing feature is that the dynamic fluctuation of electrons is separate from the electronic structure calculations such that the standard fixed-number DFT implementation in existing AIMD codes can be used with only minor modifications. The dynamics derived by using the potential energy of extended system follows correct statistics, and the generated MD trajectory samples the grand canonical ensemble at the pre-set electron chemical potential. Bouzid and Pasquarello<sup>133</sup> use this method to simulate the electrified Pt water interfaces under bias potentials but with a different potential reference scheme.

One common issue for constant potential approaches is that charge fluctuation under PBC can have spurious effects on potential reference and energetics, rendering consistent assessment of potentials and total energies difficult. Thus, calculations with fixed number of particles (i.e., canonical ensemble) have been often used in studies of interface electrochemistry. In the canonical ensemble approaches, the surface charge densities on the electrodes are controlled instead, and the corresponding electrode potentials are then calculated. In the simulation models, the charges on the electrodes need to be compensated by counter charges to keep the simulation cells neutral under PBC. The counter charges are placed near the EDL in explicit solvation models,<sup>137</sup> or described by some form of charge distribution in the implicit models.<sup>76,127,131,138</sup>

To obtain the electrode potential at a given surface charge density of the electrode, the Fermi level of the electrode needs to be aligned to a consistent reference. The implicit interface model can use the electrostatic potential of bulk electrolyte solution as reference when varying the surface charge of the electrode. As only the electrostatic effects are

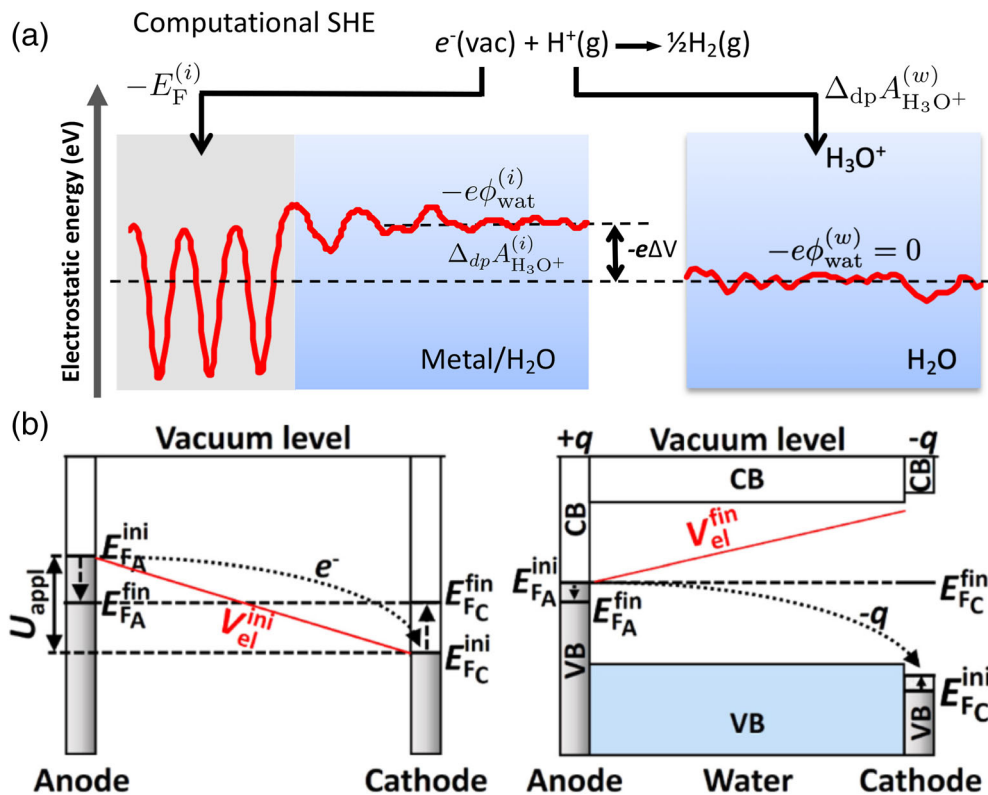


**FIGURE 7** (a) Schematic illustration of alignment of electrostatic potentials between metal/water interface model (left) and pure water model (right) in the computational standard hydrogen electrode scheme. (Reprinted with permission from Ref. 125). (b) Schematic representation of the AIMD full-cell model used to realize an electrolytic cell. The figure on the left shows the alignment between two metal electrodes before (superscript “ini”) and after (superscript “fin”) charge transfer. The figure on the right shows a doped semiconductor electrode allows for controlling the position of the Fermi level. (Reprinted with permission from Ref. 134)

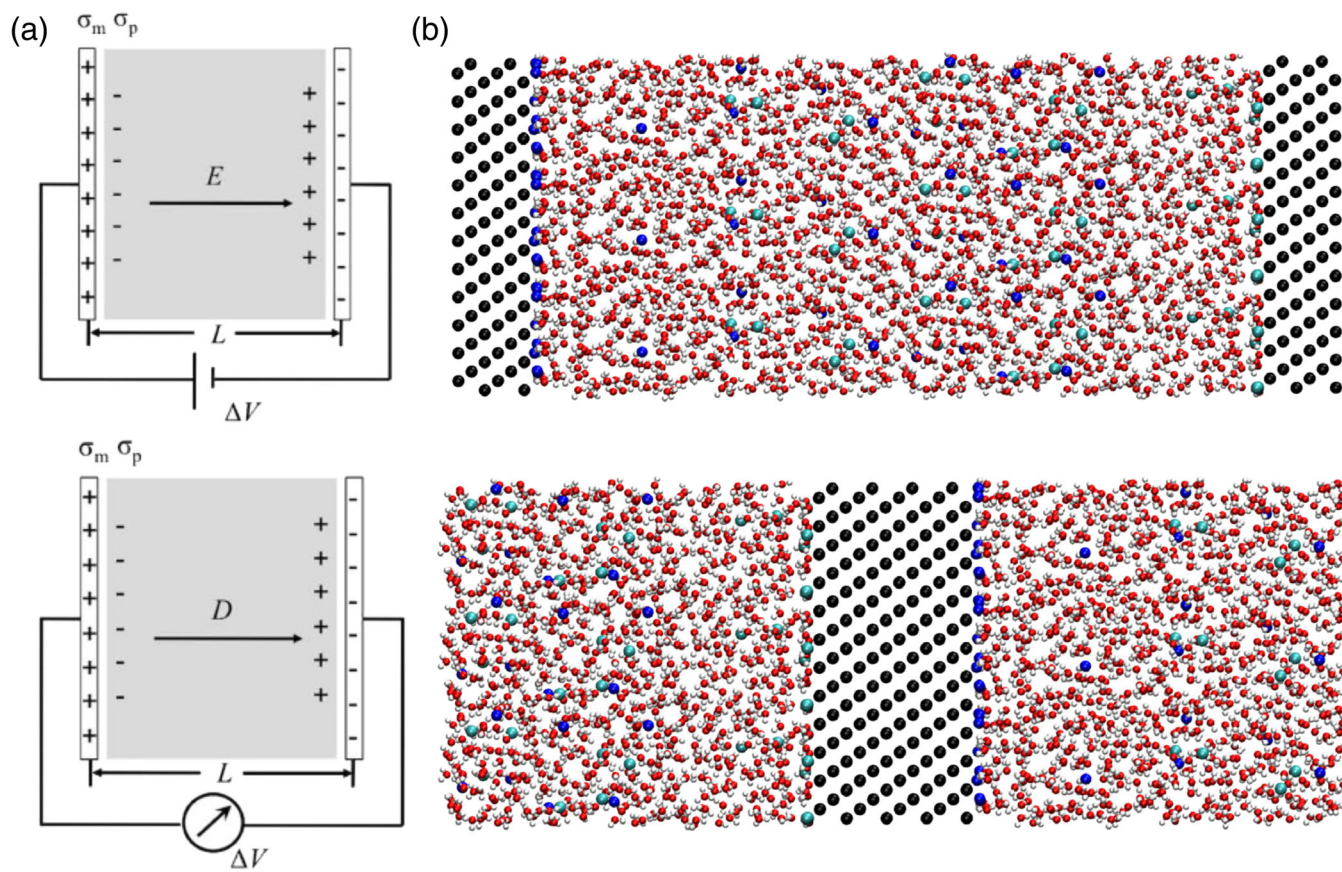


**FIGURE 8** (a) Schematic illustration of imposing finite fields in a periodic cell, as demonstrated by a parallel plate capacitor at constant electric field,  $E$ , and at constant electric displacement,  $D$ .  $\sigma_m$  is the surface charge density on the metal electrode, and  $\sigma_p$  is the polarization surface charge density of the dielectric material. (Reprinted with permission from Ref. 142). (b) Interface models of classical polarizable electrodes under applied potentials. Top: Electrolyte-centered supercell under 2D PBC, with fixed applied potential between two electrodes. Bottom: Conductor-centered supercell under 3D PBC, with a finite field and a single electrode in which all atoms are set to have the same electric potential. (Reprinted with permission from Ref. 135)

included in the implicit solvation models, the electrostatic potential of the bulk electrolyte is essentially the same as the vacuum level. Therefore, the electrode potential can be converted to the SHE scale by subtracting the absolute SHE potential (i.e., 4.44 eV according to Trasatti).

Similarly, aligning potentials in the explicit interface models also need a consistent reference. Early works such as Taylor et al.<sup>139</sup> and Duan et al.<sup>140</sup> introduced the vacuum layer in the metal/water interface model, and thus the electrostatic potential of the vacuum can be used as the reference. Same as in the implicit interface model, electrode potentials can be calculated with reference to the vacuum potential, and then converted to the SHE scale by subtracting the absolute SHE potential. Alternatively, the potential can be referenced to the SHE scale directly by subtracting the deprotonation energy of aqueous hydronium ( $\Delta_{dp}A_{H_3O^+}$ ). This scheme is presented in the Figure 7(a). The value of  $\Delta_{dp}A_{H_3O^+}^{(i)}$  for interface model and  $\Delta_{dp}A_{H_3O^+}^{(w)}$  for bulk water model are different due to the uncertainty of electrostatic potential reference under PBC. This indicates that  $\Delta_{dp}A_{H_3O^+}^{(i)}$  should be recalculated for every interface model with different chemical composition. Expensive calculation of  $\Delta_{dp}A_{H_3O^+}^{(i)}$  can be avoided by aligning the electrostatic potential of bulk solution in interface model ( $\phi_{wat}^{(i)}$ ) with its counterpart in bulk water model ( $\phi_{wat}^{(w)}$ ).<sup>125</sup> As a result, the  $\Delta_{dp}A_{H_3O^+}^{(w)}$ , which is calculated once in bulk water model, can be readily converted into  $\Delta_{dp}A_{H_3O^+}^{(i)}$  by adding the difference between  $\phi_{wat}^{(i)}$  and  $\phi_{wat}^{(w)}$ .

Finally, it is worth pointing out that equilibrium electrochemical conditions also specify constant electrochemical potentials of electrolyte ions. In half-cell models, this, in principle, also requires fluctuating numbers of ions (e.g.,  $H^+$ )

if the ions undergo chemical transformation at electrode surfaces. Computational treatment with constant electrochemical potentials of ions is still rare. A notable exception is the work of Rossmeisl et al.,<sup>141</sup> in which a generalized scheme is proposed to investigate the effects of both electrode potential and pH. They calculate a series of interface models corresponding to a variety of pH, and then employ a post-processing procedure to determine the electrode potential of each configuration, from which the grand potential is constructed.

## 5.2 | Full-cell models

In addition to the commonly used half-cell models, there are some promising methods using full-cell interface models which have been recently proposed for modeling electrified interfaces.<sup>134,142</sup> The full-cell models simulated in the canonical ensemble are effectively equivalent to the setup in electrochemical experiment. In contrast to the half-cell models, both electrochemical potentials of the electrons and electrolyte ions in the full-cell models can be kept constant without the need of changing the number of particles, as the counter electrode and bulk solution can be regarded as reservoirs for electrons and electrolyte ions, respectively. The full-cell simulations with 2D PBC were already implemented in the MM calculation.<sup>32</sup>

However, AIMD modeling of electrochemical full-cell systems faces a challenge of how to adjust the electrode potential, because the Fermi level is kept constant throughout the cell in the SCF DFT calculation (left scheme in Figure 7(b)). Consequently, no electric field is allowed between the two electrodes. In order to create a potential bias across the cell, Surendralal et al.<sup>134</sup> proposed a simulation method using a doped semiconductor (either p-type or n-type doping) with a large band gap as the counter electrode, and a dipole correction scheme to treat the potential change along surface normal direction under PBC. In this way, the charges on the metal electrode and the doped semiconductor (i.e., inert Ne electrode) are redistributed, and thus the electric field between two electrodes is generated, as presented in the right scheme of Figure 7(b). In the implementation, dopant charges are introduced by changing the nuclear charges of the Ne atoms in the semiconductor counter electrode. This method was then applied to studying the hydrogen evolution reaction (HER) that occurs during the initial corrosion of the Mg/water interface under anodic polarization.<sup>134</sup>

A finite field MD simulation method recently developed by Sprik et al. holds great promise in simulating electrified interfaces in full-cell models.<sup>143–148</sup> Finite field MD simulations adopt the constant electric field Hamiltonian introduced by Stengel, Spaldin and Vanderbilt,<sup>149</sup> in which an electric field,  $E$ , or displacement,  $D$ , acting as an electrostatic boundary condition is imposed to account for the interaction between the periodic system with the fixed field, as illustrated in Figure 8(a). Through computing the polarization of the full periodic cell during MD simulations, one can derive the electrical properties such as dielectric constants and EDL capacitances. Zhang and Sprik tested the method in a simple point charge model consisting of a NaCl aqueous solution confined between two oppositely charged walls,<sup>143</sup> and later applied it to simulation of the interface between a polar NaCl crystal slab and a NaCl aqueous solution.<sup>144–146</sup> Using constant,  $D$ , MD simulation, they were also able to calculate the dielectric constant of liquid water at increased speed of convergence.<sup>147</sup> These calculations were performed based on the classical force field models, and the first application with AIMD was modeling electrified semiconducting TiO<sub>2</sub> water interfaces to calculate the capacitances of the Helmholtz double layer at acidic and alkaline conditions.<sup>148</sup> Note that in all the above mentioned studies at both MM and QM level, the electrode surfaces are non-polarizable, in the sense that the net surface charges are fixed during MD simulations, even for the QM models of semiconductor TiO<sub>2</sub> surfaces charged by protons, not electrons.

The ideal would also be to extend the finite field MD method to simulate metallic electrodes that can be polarized with induced charges under applied potentials or fields. In a full PBC cell, the presence of the finite field can polarize a single metallic slab immersed in electrolyte solution such that the two surfaces of the slab are induced with opposite charges, leading to a potential drop at the two electrode/electrolyte interfaces. This amounts to a full-cell setup with the two short-wired surfaces of a single electrode slab, simultaneously representing both the cathode and anode in an electrochemical cell. Combining the classical polarizable electrode model enabled by the Siepmann-Sprik potential, Salanne, Sprik, and co-workers implemented the finite field MD method to model metallic electrodes in contact with an aqueous ionic solution at a constant potential.<sup>135</sup> They validated this attractive approach by showing the polarization of the single metallic slab with correct charge distribution compared with the results obtained from an early 2D PBC implementation, as illustrated in Figure 8(b). This advance opens a promising way to modeling electrochemical interfaces at controlled potentials or fields. Note that the finite field AIMD has yet to be applied to metallic systems so far due to various technical difficulties.

## 6 | CONCLUSION AND OUTLOOK

This review introduces a variety of computational methods used for electrochemical simulation. We first summarize a variety of choices of energy models for multiscale simulations, ranging from quantum mechanical, molecular mechanical, to coarse grained and continuum models. We then introduce some applications of various models and their combinations for targeted problems in solution and interface electrochemistry. In interface electrochemistry, we stress that water chemisorption can have a significant impact in determining electrode potentials and EDL capacitances, particularly on active electrode surfaces. In these cases, AIMD can serve as good benchmark for the development of efficient multiscale embedding schemes. Furthermore, we discuss the methods of controlling electrode potentials for both half-cell models and full-cell models. In the half-cell mode, enforcing constant potential in simulation requires sophisticated grand canonical ensemble approaches, which can be implemented at either the SCF DFT level or MD level. Alternatively, one can use a “sample and measure” approach, in which a series of electrified interface models with different surface charge densities are constructed in separate, and then the corresponding electrode potentials are calculated afterward with each DFT calculation performed with fixed number of particles. On the other hand, the full-cell mode resembles the experimental setup, and the electrochemical potentials of electrons and ions can be applied without the need of changing the number of particles in periodic cells. Some early implementations, i.e. the finite field MD method at both classical and quantum mechanical level, have demonstrated that the full-cell models are a very promising approach for modeling electrochemical interfaces.

During the last decade, machine learning (ML) methods have been changing our simulation protocols.<sup>150–154</sup> Fitting quantum mechanical calculation data, the ML models can accurately reproduce potential energy surfaces, allowing for much faster sampling of configurational space with ab initio accuracy. The latest development of Deep Potentials (DP) can speed up the AIMD calculation by the stunning  $10^6$ – $10^8$  times.<sup>152–154</sup> This certainly gives us the hope for modeling realistic electrochemical cells at the accuracy of quantum mechanical level, in particular combining the DP models with finite field MD in a full-cell mode. However, the ML potentials rely on local representation of atomic environment, which may be inappropriate for treating long range electrostatic interactions that are essential in electrochemistry. Thus, the first hurdle to overcome is how to effectively incorporate long range electrostatic interactions in the ML potentials.<sup>155</sup> When combining with finite field MD, the ML potentials also need to include field response.

## ACKNOWLEDGMENT

We are grateful for funding support from the National Natural Science Foundation of China (Grants Nos 21861132015, 21991151, 21991150, 22021001, and 91745103).

## CONFLICT OF INTEREST

The authors have declared no conflicts of interest for this article.

## AUTHOR CONTRIBUTIONS

**Xiao-Hui Yang:** Investigation; visualization; writing-original draft; writing-review & editing. **Yong-Bin Zhuang:** Investigation; writing-review & editing. **Jia-Xin Zhu:** Investigation; writing-review & editing. **Jia-Bo Le:** Writing-review & editing. **Jun Cheng:** Conceptualization; project administration; supervision; writing-original draft; writing-review & editing.

## DATA AVAILABILITY STATEMENT

Data sharing is not applicable to this article as no new data were created or analyzed in this study.

## ORCID

Xiao-Hui Yang  <https://orcid.org/0000-0002-5652-6621>

Yong-Bin Zhuang  <https://orcid.org/0000-0001-5182-8084>

Jia-Xin Zhu  <https://orcid.org/0000-0002-3471-4728>

Jun Cheng  <https://orcid.org/0000-0001-6971-0797>

## ENDNOTES

\* The Siepmann-Sprik potential has been implemented in the Lammps program (<https://github.com/zhenxingwang/lammps-conp>) and the MetalWalls program (<https://gitlab.com/ampere2/metalwalls>).

<sup>†</sup> Implicit solvation models can be found in the following quantum chemistry codes: PCM and SMD are recommended by Gaussian16 program (<http://gaussian.com/scrf/?tabid=7>) for continuous representation of solvent effect, COSMO is implemented in TURBOMOLE program (<https://www.turbomole.org/>) or nwchem program (<https://www.nwchem-sw.org/>), and the implementation of SMx family can also be found at the website <https://comp.chem.umn.edu/solvation/comparison.htm>.

## RELATED WIRES ARTICLE

[Atomistic modeling of electrocatalysis: Are we there yet?](#)

## REFERENCES

1. Li C-Y, Le J-B, Wang Y-H, Chen S, Yang Z-L, Li J-F, et al. In situ probing electrified interfacial water structures at atomically flat surfaces. *Nat Mater.* 2019;18:697–701. <https://doi.org/10.1038/s41563-019-0356-x>
2. Singh MR, Kwon Y, Lum Y, Ager JW, Bell AT. Hydrolysis of electrolyte cations enhances the electrochemical reduction of CO<sub>2</sub> over ag and cu. *J Am Chem Soc.* 2016;138:13006–12. <https://doi.org/10.1021/jacs.6b07612>
3. Yin Z, Peng H, Wei X, Zhou H, Gong J, Huai M, et al. An alkaline polymer electrolyte CO<sub>2</sub> electrolyzer operated with pure water. *Energy Environ Sci.* 2019;12:2455–62. <https://doi.org/10.1039/c9ee01204d>
4. Lim H-K, Kwon Y, Kim HS, Jeon J, Kim Y-H, Lim J-A, et al. Insight into the microenvironments of the metal–ionic liquid interface during electrochemical CO<sub>2</sub> reduction. *ACS Catal.* 2018;8:2420–7. <https://doi.org/10.1021/acscatal.7b03777>
5. Le J-B, Fan Q-Y, Li J-Q, Cheng J. Molecular origin of negative component of Helmholtz capacitance at electrified Pt(111)/water interface. *Sci Adv.* 2020;6(41):eabb1219. <https://doi.org/10.1126/sciadv.abb1219>
6. Hummer G, Pratt LR, García AE. Free energy of ionic hydration. *J Phys Chem.* 1996;100:1206–15. <https://doi.org/10.1021/jp951011v>
7. Merlet C, Rotenberg B, Madden PA, Taberna P-L, Simon P, Gogotsi Y, et al. On the molecular origin of supercapacitance in nanoporous carbon electrodes. *Nat Mater.* 2012;11:306–10. <https://doi.org/10.1038/nmat3260>
8. Gartner TE, Jayaraman A. Modeling and simulations of polymers: a roadmap. *Macromolecules.* 2019;52:755–86. <https://doi.org/10.1021/acs.macromol.8b01836>
9. Hummer G, Pratt LR, Garcia AE. Hydration free energy of water. *J Phys Chem.* 1995;99:14188–94. <https://doi.org/10.1021/j100038a062>
10. Tannor DJ, Marten B, Murphy R, Friesner RA, Sitkoff D, Nicholls A, et al. Accurate first principles calculation of molecular charge distributions and solvation energies from ab initio quantum mechanics and continuum dielectric theory. *J Am Chem Soc.* 1994;116:11875–82. <https://doi.org/10.1021/ja00105a030>
11. Kelly CP, Cramer CJ, Truhlar DG. Single-ion solvation free energies and the Normal hydrogen electrode potential in methanol, acetonitrile, and dimethyl sulfoxide. *J Phys Chem B.* 2007;111:408–22. <https://doi.org/10.1021/jp065403l>
12. Andreussi O, Dabo I, Marzari N. Revised self-consistent continuum solvation in electronic-structure calculations. *J Chem Phys.* 2012;136:064102. <https://doi.org/10.1063/1.3676407>
13. McGrath MJ, Kuo I-FW, Ngouana W, Ghogomu JN, Mundy CJ, Marenich AV, et al. Calculation of the Gibbs free energy of solvation and dissociation of HCl in water via Monte Carlo simulations and continuum solvation models. *Phys Chem Chem Phys.* 2013;15:13578. <https://doi.org/10.1039/c3cp51762d>
14. Ambrosio F, Guo Z, Pasquarello A. Absolute energy levels of liquid water. *J Phys Chem Lett.* 2018;9:3212–6. <https://doi.org/10.1021/acs.jpclett.8b00891>
15. Ansari N, Karmakar T, Parrinello M. Molecular mechanism of gas solubility in liquid: constant chemical potential molecular dynamics simulations. *J Chem Theory Comput.* 2020;16:5279–86. <https://doi.org/10.1021/acs.jctc.0c00450>
16. Cheng J, Sulpizi M, Sprik M. Redox potentials and pKa for benzoquinone from density functional theory based molecular dynamics. *J Chem Phys.* 2009;131:154504. <https://doi.org/10.1063/1.3250438>
17. Keith JA, Carter EA. Theoretical insights into pyridinium-based photoelectrocatalytic reduction of CO<sub>2</sub>. *J Am Chem Soc.* 2012;134:7580–3. <https://doi.org/10.1021/ja300128e>
18. Marenich AV, Ho J, Coote ML, Cramer CJ, Truhlar DG. Computational electrochemistry: prediction of liquid-phase reduction potentials. *Phys Chem Chem Phys.* 2014;16:15068–106. <https://doi.org/10.1039/c4cp01572j>
19. Cheng J, Liu X, VandeVondele J, Sulpizi M, Sprik M. Redox potentials and acidity constants from density functional theory based molecular dynamics. *Acc Chem Res.* 2014;47:3522–9. <https://doi.org/10.1021/ar500268y>
20. Shen L, Yang W. Quantum mechanics/molecular mechanics method combined with hybrid all-atom and coarse-grained model: theory and application on redox potential calculations. *J Chem Theory Comput.* 2016;12:2017–27. <https://doi.org/10.1021/acs.jctc.5b01107>
21. Salvo JLD, Luca GD, Cipollina A, Micale G. Effect of ion exchange capacity and water uptake on hydroxide transport in PSU-TMA membranes: a DFT and molecular dynamics study. *J Membr Sci.* 2020;599:117837.
22. Chen LD, Urushihara M, Chan K, Nørskov JK. Electric field effects in electrochemical CO<sub>2</sub> reduction. *ACS Catal.* 2016;6:7133–9. <https://doi.org/10.1021/acscatal.6b02299>
23. Bagger A, Ju W, Varela AS, Strasser P, Rossmeisl J. Electrochemical CO<sub>2</sub> reduction: a classification problem. *ChemPhysChem.* 2017;18:3266–73. <https://doi.org/10.1002/cphc.201700736>

24. Grimme S, Bannwarth C, Shushkov P. A robust and accurate tight-binding quantum chemical method for structures, vibrational frequencies, and noncovalent interactions of large molecular systems parametrized for all spd-block elements ( $Z = 1\text{--}86$ ). *J Chem Theory Comput.* 2017;13:1989–2009. <https://doi.org/10.1021/acs.jctc.7b00118>
25. Gaus M, Cui Q, Elstner M. DFTB3: extension of the self-consistent-charge density-functional tight-binding method (SCC-DFTB). *J Chem Theory Comput.* 2011;7:931–48. <https://doi.org/10.1021/ct100684s>
26. Perlt E, Ray P, Hansen A, Malberg F, Grimme S, Kirchner B. Finding the best density functional approximation to describe interaction energies and structures of ionic liquids in molecular dynamics studies. *J Chem Phys.* 2018;148:193835. <https://doi.org/10.1063/1.5013122>
27. Jorgensen WL, Maxwell DS, Tirado-Rives J. Development and testing of the OPLS all-atom force field on conformational energetics and properties of organic liquids. *J Am Chem Soc.* 1996;118:11225–36. <https://doi.org/10.1021/ja9621760>
28. Bulo RE, Michel C, Fleurat-Lessard P, Sautet P. Multiscale modeling of chemistry in water: are we there yet? *J Chem Theory Comput.* 2013;9:5567–77. <https://doi.org/10.1021/ct4005596>
29. Mitchell PJ, Fincham D. Shell model simulations by adiabatic dynamics. *J Phys Condens Matter.* 1993;5:1031–8. <https://doi.org/10.1088/0953-8984/5/8/006>
30. Geada IL, Ramezani-Dakhel H, Jamil T, Sulpizi M, Heinz H. Insight into induced charges at metal surfaces and biointerfaces using a polarizable Lennard-Jones potential. *Nat Commun.* 2018;9(1):716. <https://doi.org/10.1038/s41467-018-03137-8>
31. Siepmann JI, Sprik M. Influence of surface topology and electrostatic potential on water/electrode systems. *J Chem Phys.* 1995;102:511–24. <https://doi.org/10.1063/1.469429>
32. Reed SK, Lanning OJ, Madden PA. Electrochemical interface between an ionic liquid and a model metallic electrode. *J Chem Phys.* 2007;126:084704. <https://doi.org/10.1063/1.2464084>
33. van Duin ACT, Dasgupta S, Lorant F, Goddard WA. ReaxFF: a reactive force field for hydrocarbons. *J Phys Chem A.* 2001;105:9396–409. <https://doi.org/10.1021/jp004368u>
34. Åqvist J, Warshel A. Simulation of enzyme reactions using valence bond force fields and other hybrid quantum/classical approaches. *Chem Rev.* 1993;93:2523–44. <https://doi.org/10.1021/cr00023a010>
35. Lobaugh J, Voth GA. The quantum dynamics of an excess proton in water. *J Chem Phys.* 1996;104:2056–69. <https://doi.org/10.1063/1.470962>
36. Day TJF, Soudackov AV, Čuma M, Schmitt UW, Voth GA. A second generation multistate empirical valence bond model for proton transport in aqueous systems. *J Chem Phys.* 2002;117:5839–49. <https://doi.org/10.1063/1.1497157>
37. Tse Y-LS, Sarode HN, Lindberg GE, Witten TA, Yang Y, Herring AM, et al. Chloride enhances fluoride mobility in anion exchange membrane/polycationic systems. *J Phys Chem C.* 2013;118:845–53. <https://doi.org/10.1021/jp409728a>
38. Chen C, Tse Y-LS, Lindberg GE, Knight C, Voth GA. Hydroxide solvation and transport in anion exchange membranes. *J Am Chem Soc.* 2016;138:991–1000. <https://doi.org/10.1021/jacs.5b11951>
39. Li J-Q, Meng L, Sprik M, Cheng J. Thermodynamic investigation of proton/electron interplay on the Pourbaix diagram at the TiO<sub>2</sub>/electrolyte interface. *J Phys Chem C.* 2020;124:19003–14. <https://doi.org/10.1021/acs.jpcc.0c03546>
40. Chen S, Wang H, Zhang J, Lu S, Xiang Y. Effect of side chain on the electrochemical performance of poly (ether ether ketone) based anion-exchange membrane: a molecular dynamics study. *J Membr Sci.* 2020;605:118105. <https://doi.org/10.1016/j.memsci.2020.118105>
41. Miertuš S, Scrocco E, Tomasi J. Electrostatic interaction of a solute with a continuum. A direct utilization of AB initio molecular potentials for the prediction of solvent effects. *Chem Phys.* 1981;55:117–29. [https://doi.org/10.1016/0301-0104\(81\)85090-2](https://doi.org/10.1016/0301-0104(81)85090-2)
42. Chuev GN, Chioldo S, Erofeeva SE, Fedorov MV, Russo N, Sicilia E. A quasilinear RISM approach for the computation of solvation free energy of ionic species. *Chem Phys Lett.* 2006;418:485–9. <https://doi.org/10.1016/j.cplett.2005.10.117>
43. Petrosyan SA, Rigos AA, Arias TA. Joint density-functional theory: ab initio study of Cr<sub>2</sub>O<sub>3</sub>Surface chemistry in solution. *J Phys Chem B.* 2005;109:15436–44. <https://doi.org/10.1021/jp044822k>
44. Schwarz K, Sundararaman R. The electrochemical interface in first-principles calculations. *Surf Sci Rep.* 2020;75:100492. <https://doi.org/10.1016/j.surfrept.2020.100492>
45. Bonaccorsi R, Scrocco E, Tomasi J. Molecular SCF calculations for the ground state of some three-membered ring molecules: (CH<sub>2</sub>)<sub>3</sub>, (CH<sub>2</sub>)<sub>2</sub>NH, (CH<sub>2</sub>)<sub>2</sub>NH<sub>2</sub><sup>+</sup>, (CH<sub>2</sub>)<sub>2</sub>O, (CH<sub>2</sub>)<sub>2</sub>S, (CH<sub>2</sub>)<sub>2</sub>CH<sub>2</sub>, and N<sub>2</sub>CH<sub>2</sub>. *J Chem Phys.* 1970;52:5270–84. <https://doi.org/10.1063/1.1672775>
46. Tomasi J, Persico M. Molecular interactions in solution: an overview of methods based on continuous distributions of the solvent. *Chem Rev.* 1994;94:2027–94. <https://doi.org/10.1021/cr00031a013>
47. Tomasi J, Mennucci B, Cammi R. Quantum mechanical continuum solvation models. *Chem Rev.* 2005;105:2999–3094. <https://doi.org/10.1021/cr9904009>
48. Floris F, Tomasi J. Evaluation of the dispersion contribution to the solvation energy. A simple computational model in the continuum approximation. *J Comput Chem.* 1989;10:616–27. <https://doi.org/10.1002/jcc.540100504>
49. Grant JA, Williams RL, Scheraga HA. Ab initio self-consistent field and potential-dependent partial equalization of orbital electronegativity calculations of hydration properties of N-acetyl-N<sup>?</sup>-methyl-alanineamide. *Biopolymers.* 1990;30:929–49. <https://doi.org/10.1002/bip.360300908>
50. Bajorath J, Kraut J, Li ZQ, Kitson DH, Hagler AT. Theoretical studies on the dihydrofolate reductase mechanism: electronic polarization of bound substrates. *Proc Natl Acad Sci U S A.* 1991;88:6423–6. <https://doi.org/10.1073/pnas.88.15.6423>
51. Miertus S, Freer V. Continuum models of environmental effects on molecular structure and mechanisms in chemistry and biology. *J Math Chem.* 1992;10:183–204. <https://doi.org/10.1007/bf01169174>

52. Klamt A, Schüürmann G. COSMO: a new approach to dielectric screening in solvents with explicit expressions for the screening energy and its gradient. *J Chem Soc, Perkin Trans 2*. 1993;2:799–805. <https://doi.org/10.1039/p29930000799>
53. Cramer CJ, Truhlar DG. Implicit solvation models: equilibria, structure, spectra, and dynamics. *Chem Rev*. 1999;99:2161–200. <https://doi.org/10.1021/cr960149m>
54. Marenich AV, Olson RM, Kelly CP, Cramer CJ, Truhlar DG. Self-consistent reaction field model for aqueous and nonaqueous solutions based on accurate polarized partial charges. *J Chem Theory Comput*. 2007;3:2011–33. <https://doi.org/10.1021/ct7001418>
55. Amovilli C, Barone V, Cammi R, Cancès E, Cossi M, Mennucci B, et al. Advances in quantum chemistry. *Adv Quantum Chem*. 1998; 32:227–61.
56. Fattebert J-L, Gygi F. Density functional theory for efficient ab initio molecular dynamics simulations in solution. *J Comput Chem*. 2002;23:662–6. <https://doi.org/10.1002/jcc.10069>
57. Scherlis DA, Fattebert J-L, Gygi F, Cococcioni M, Marzari N. A unified electrostatic and cavitation model for first-principles molecular dynamics in solution. *J Chem Phys*. 2006;124:074103. <https://doi.org/10.1063/1.2168456>
58. Fisicaro G, Genovese L, Andreussi O, Mandal S, Nair NN, Marzari N, et al. Soft-sphere continuum solvation in electronic-structure calculations. *J Chem Theory Comput*. 2017;13:3829–45. <https://doi.org/10.1021/acs.jctc.7b00375>
59. Sundararaman R, Letchworth-Weaver K, Schwarz KA. Improving accuracy of electrochemical capacitance and solvation energetics in first-principles calculations. *J Chem Phys*. 2018;148:144105. <https://doi.org/10.1063/1.5024219>
60. Dupont C, Andreussi O, Marzari N. Self-consistent continuum solvation (SCCS): the case of charged systems. *J Chem Phys*. 2013;139: 214110. <https://doi.org/10.1063/1.4832475>
61. Scalmani G, Frisch MJ. Continuous surface charge polarizable continuum models of solvation. I General formalism. *J Chem Phys*. 2010;132:114110.
62. Miguel ELM, Silva PL, Pliego JR. Theoretical prediction of pKa in methanol: testing SM8 and SMD models for carboxylic acids, phenols, and amines. *J Phys Chem B*. 2014;118:5730–9. <https://doi.org/10.1021/jp501379p>
63. Dutra FR, Silva Cde S, Custodio R. On the accuracy of the direct method to calculate pKa from electronic structure calculations. *J Phys Chem A*. 2020;125:65–73. <https://doi.org/10.1021/acs.jpca.0c08283>
64. Nam KW, Kim H, Beldjoudi Y, Kwon TW, Kim DJ, Stoddart JF. Redox-active Phenanthrenequinone triangles in aqueous rechargeable zinc batteries. *J Am Chem Soc*. 2020;142:2541–8. <https://doi.org/10.1021/jacs.9b12436>
65. Malakar T, Hanson CS, Devery JJ, Zimmerman PM. Combined theoretical and experimental investigation of Lewis acid-carbonyl interactions for metathesis. *ACS Catal*. 2021;11:4381–94. <https://doi.org/10.1021/acscatal.0c05277>
66. Srnec M, Iyer SR, Dassama LMK, Park K, Wong SD, Sutherlin KD, et al. Nuclear resonance vibrational spectroscopic definition of the facial triad FeIV=O intermediate in taurine dioxygenase: evaluation of structural contributions to hydrogen atom abstraction. *J Am Chem Soc*. 2020;142:18886–96.
67. Tomaník L, Muchová E, Slavíček P. Solvation energies of ions with ensemble cluster-continuum approach. *Phys Chem Chem Phys*. 2020;22:22357–68. <https://doi.org/10.1039/d0cp02768e>
68. Kurtz DA, Dhar D, Elgrishi N, Kandemir B, McWilliams SF, Howland WC, et al. Redox-induced structural reorganization dictates kinetics of cobalt(III) hydride formation via proton-coupled electron transfer. *J Am Chem Soc*. 2021;143:3393–406. <https://doi.org/10.1021/jacs.0c11992>
69. Bamford KL, Qu ZW, Stephan DW. Reactions of B 2 ( o -tolyl) 4 with boranes: assembly of the Pentaborane(9), HB[B(o-tolyl)( $\mu$ -H)] 4. *Angew Chem Int Ed*. 2021;60:8532–6. <https://doi.org/10.1002/anie.202101054>
70. Andreussi O, Marzari N. Electrostatics of solvated systems in periodic boundary conditions. *Phys Rev B*. 2014;90:245101. <https://doi.org/10.1103/physrevb.90.245101>
71. Andreussi O, Hörmann NG, Nattino F, Fisicaro G, Goedecker S, Marzari N. Solvent-aware interfaces in continuum solvation. *J Chem Theory Comput*. 2019;15:1996–2009. <https://doi.org/10.1021/acs.jctc.8b01174>
72. Letchworth-Weaver K, Arias TA. Joint density functional theory of the electrode-electrolyte interface: application to fixed electrode potentials, interfacial capacitances, and potentials of zero charge. *Phys Rev B*. 2012;86:075140. <https://doi.org/10.1103/physrevb.86.075140>
73. Nishihara S, Otani M. Hybrid solvation models for bulk, interface, and membrane: reference interaction site methods coupled with density functional theory. *Phys Rev B*. 2017;96:115429. <https://doi.org/10.1103/physrevb.96.115429>
74. Chandler D, McCoy JD, Singer SJ. Density functional theory of nonuniform polyatomic systems. I. General formulation. *J Chem Phys*. 1986;85:5971–6. <https://doi.org/10.1063/1.451510>
75. Chandler D, McCoy JD, Singer SJ. Density functional theory of nonuniform polyatomic systems. II. Rational closures for integral equations. *J Chem Phys*. 1986;85:5977–82. <https://doi.org/10.1063/1.451511>
76. Haruyama J, Ikeshoji T, Otani M. Electrode potential from density functional theory calculations combined with implicit solvation theory. *Phys Rev Mater*. 2018;2:095801. <https://doi.org/10.1103/physrevmaterials.2.095801>
77. Petrosyan SA, Briere J-F, Roundy D, Arias TA. Joint density-functional theory for electronic structure of solvated systems. *Phys Rev B*. 2007;75:205105. <https://doi.org/10.1103/physrevb.75.205105>
78. Sundararaman R, Letchworth-Weaver K, Arias TA. A recipe for free-energy functionals of polarizable molecular fluids. *J Chem Phys*. 2014;140:144504. <https://doi.org/10.1063/1.4870653>
79. Sundararaman R, Gunceler D, Arias TA. Weighted-density functionals for cavity formation and dispersion energies in continuum solvation models. *J Chem Phys*. 2014;141:134105. <https://doi.org/10.1063/1.4896827>

80. Kovalenko A, Hirata F. Three-dimensional density profiles of water in contact with a solute of arbitrary shape: a RISM approach. *Chem Phys Lett.* 1998;290:237–44. [https://doi.org/10.1016/s0009-2614\(98\)00471-0](https://doi.org/10.1016/s0009-2614(98)00471-0)
81. Sato H, Kovalenko A, Hirata F. Self-consistent field, ab initio molecular orbital and three-dimensional reference interaction site model study for solvation effect on carbon monoxide in aqueous solution. *J Chem Phys.* 2000;112:9463–8. <https://doi.org/10.1063/1.481564>
82. Kondrat S, Georgi N, Fedorov MV, Kornyshev AA. A superionic state in nano-porous double-layer capacitors: insights from Monte Carlo simulations. *Phys Chem Chem Phys.* 2011;13:11359. <https://doi.org/10.1039/c1cp20798a>
83. Sun Y, Kollman PA. Hydrophobic solvation of methane and nonbond parameters of the TIP3P water model. *J Comput Chem.* 1995;16: 1164–9. <https://doi.org/10.1002/jcc.540160910>
84. Leung K, Rempe SB, Lilienfeld OA. Ab initio molecular dynamics calculations of ion hydration free energies. *J Chem Phys.* 2009;130: 204507. <https://doi.org/10.1063/1.3137054>
85. Li G, Zhang X, Cui Q. Free energy perturbation calculations with combined QM/MM potentials complications, simplifications, and applications to redox potential calculations. *J Phys Chem B.* 2003;107:8643–53. <https://doi.org/10.1021/jp034286g>
86. Riccardi D, Schaefer P, Cui Q. pKaCalculations in solution and proteins with QM/MM free energy perturbation simulations: a quantitative test of QM/MM protocols. *J Phys Chem B.* 2005;109:17715–33. <https://doi.org/10.1021/jp0517192>
87. Ayala R, Sprik M. A classical point charge model study of system size dependence of oxidation and reorganization free energies in aqueous solution. *J Phys Chem B.* 2008;112:257–69. <https://doi.org/10.1021/jp0748516>
88. Costanzo F, Sulpizi M, Valle RGD, Sprik M. The oxidation of tyrosine and tryptophan studied by a molecular dynamics normal hydrogen electrode. *J Chem Phys.* 2011;134:244508. <https://doi.org/10.1063/1.3597603>
89. Cheng J, Sprik M. Aligning electronic energy levels at the TiO<sub>2</sub>/H<sub>2</sub>O interface. *Phys Rev B.* 2010;82(8):081406. <https://doi.org/10.1103/physrevb.82.081406>
90. Cheng J, Sprik M. Alignment of electronic energy levels at electrochemical interfaces. *Phys Chem Chem Phys.* 2012;14:11245. <https://doi.org/10.1039/c2cp41652b>
91. Cheng J, Liu X, Kattirtzi JA, VandeVondele J, Sprik M. Aligning electronic and protonic energy levels of proton-coupled electron transfer in water oxidation on aqueous TiO<sub>2</sub>. *Angew Chem Int Ed.* 2014;53:12046–50. <https://doi.org/10.1002/anie.201405648>
92. Yang X-H, Cuesta A, Cheng J. Computational ag/AgCl reference electrode from density functional theory-based molecular dynamics. *J Phys Chem B.* 2019;123:10224–32. <https://doi.org/10.1021/acs.jpcb.9b06650>
93. Cheng J, VandeVondele J. Calculation of electrochemical energy levels in water using the random phase approximation and a double hybrid functional. *Phys Rev Lett.* 2016;116:086402. <https://doi.org/10.1103/physrevlett.116.086402>
94. Wang L-P, Van Voorhis T. A polarizable QM/MM explicit solvent model for computational electrochemistry in water. *J Chem Theory Comput.* 2012;8:610–7. <https://doi.org/10.1021/ct200340x>
95. Pezeshki S, Lin H. Recent developments in QM/MM methods towards open-boundary multi-scale simulations. *Mol Simulat.* 2014;41: 168–89. <https://doi.org/10.1080/08927022.2014.911870>
96. Laino T, Mohamed F, Laio A, Parrinello M. An efficient real space multigrid QM/MM electrostatic coupling. *J Chem Theory Comput.* 2005;1:1176–84. <https://doi.org/10.1021/ct050123f>
97. Sanchez ML, Aguilar MA, del Valle FJO. Study of solvent effects by means of averaged solvent electrostatic potentials obtained from molecular dynamics data. *J Comput Chem.* 1997;18:313–22. [https://doi.org/10.1002/\(sici\)1096-987x\(199702\)18:3<313::aid-jcc2>3.0.co;2-x](https://doi.org/10.1002/(sici)1096-987x(199702)18:3<313::aid-jcc2>3.0.co;2-x)
98. Nam K, Gao J, York DM. An efficient linear-scaling Ewald method for long-range electrostatic interactions in combined QM/MM calculations. *J Chem Theory Comput.* 2004;1:2–13. <https://doi.org/10.1021/ct049941i>
99. Nakano H, Yamamoto T. Accurate and efficient treatment of continuous solute charge density in the mean-field QM/MM free energy calculation. *J Chem Theory Comput.* 2012;9:188–203. <https://doi.org/10.1021/ct300831t>
100. Shen L, Zeng X, Hu H, Hu X, Yang W. Accurate quantum mechanical/molecular mechanical calculations of reduction potentials in Azurin variants. *J Chem Theory Comput.* 2018;14:4948–57. <https://doi.org/10.1021/acs.jctc.8b00403>
101. Stecher T, Reuter K, Oberhofer H. First-principles free-energy barriers for Photoelectrochemical surface reactions: proton abstraction at TiO<sub>2</sub>(110). *Phys Rev Lett.* 2016;117(27):276001. <https://doi.org/10.1103/physrevlett.117.276001>
102. Lim H-K, Lee H, Kim H. A seamless grid-based Interface for mean-field QM/MM coupled with efficient solvation free energy calculations. *J Chem Theory Comput.* 2016;12:5088–99. <https://doi.org/10.1021/acs.jctc.6b00469>
103. Rowley CN, Benoit R. The solvation structure of Na<sup>+</sup> and K<sup>+</sup> in liquid water determined from high level ab initio molecular dynamics simulations. *J Chem Theory Comput.* 2012;8:3526–35. <https://doi.org/10.1021/ct300091w>
104. Shiga M, Masia M. Boundary based on exchange symmetry theory for multilevel simulations. I. Basic theory. *J Chem Phys.* 2013;139: 044120. <https://doi.org/10.1063/1.4816629>
105. Boereboom JM, Potestio R, Donadio D, Bulo RE. Toward Hamiltonian adaptive QM/MM: accurate solvent structures using many-body potentials. *J Chem Theory Comput.* 2016;12:3441–8. <https://doi.org/10.1021/acs.jctc.6b00205>
106. Duster AW, Wang C-H, Garza CM, Miller DE, Lin H. Adaptive quantum/molecular mechanics: what have we learned, where are we, and where do we go from here?. *WIREs Comput Mol Sci.* 2017;7:e1310. <https://doi.org/10.1002/wcms.1310>
107. Zeng X, Hu H, Hu X, Cohen AJ, Yang W. Ab initio quantum mechanical/molecular mechanical simulation of electron transfer process: fractional electron approach. *J Chem Phys.* 2008;128:124510. <https://doi.org/10.1063/1.2832946>
108. Zeng X, Hu H, Hu X, Yang W. Calculating solution redox free energies withab initioquantum mechanical/molecular mechanical minimum free energy path method. *J Chem Phys.* 2009;130:164111. <https://doi.org/10.1063/1.3120605>

109. Brüssel M, Brehm M, Voigt T, Kirchner B. Ab initio molecular dynamics simulations of a binary system of ionic liquids. *Phys Chem Chem Phys*. 2011;13:13617. <https://doi.org/10.1039/c1cp21550g>
110. Dong D, Zhang W, van Duin ACT, Bedrov D. Grotthuss versus vehicular transport of hydroxide in anion-exchange membranes: insight from combined reactive and nonreactive molecular simulations. *J Phys Chem Lett*. 2018;9:825–9. <https://doi.org/10.1021/acs.jpclett.8b00004>
111. Wu Y, Chen H, Wang F, Paesani F, Voth GA. An improved multistate empirical valence bond model for aqueous proton solvation and transport. *J Phys Chem B*. 2008;112:467–82. <https://doi.org/10.1021/jp076658h>
112. Chen M, Zheng L, Santra B, Ko H-Y, DiStasio RA Jr, Klein ML, et al. Hydroxide diffuses slower than hydronium in water because its solvated structure inhibits correlated proton transfer. *Nat Chem*. 2018;10:413–9. <https://doi.org/10.1038/s41557-018-0010-2>
113. Chen C, Arntsen C, Tse Y-LS. Simulation study of the effects of phase separation on hydroxide solvation and transport in anion exchange membranes. *J Chem Phys*. 2020;152:094903. <https://doi.org/10.1063/1.5143168>
114. Pan J, Chen C, Li Y, Wang L, Tan L, Li G, et al. Constructing ionic highway in alkaline polymer electrolytes. *Energy Environ Sci*. 2014;7:354–60. <https://doi.org/10.1039/c3ee43275k>
115. Sinit斯基 AV, Voth GA. Quantum mechanics/coarse-grained molecular mechanics (QM/CG-MM). *J Chem Phys*. 2018;148:014102. <https://doi.org/10.1063/1.5006810>
116. Machado MR, Zeida A, Darré L, Pantano S. From quantum to subcellular scales: multi-scale simulation approaches and the SIRAH force field. *Interface Focus*. 2019;9:20180085. <https://doi.org/10.1098/rsfs.2018.0085>
117. Mironenko AV, Voth GA. Density functional theory-based quantum mechanics/coarse-grained molecular mechanics: theory and implementation. *J Chem Theory Comput*. 2020;16:6329–42. <https://doi.org/10.1021/acs.jctc.0c00751>
118. Friedrichs M, Zhou R, Edinger SR, Friesner RA. Poisson–Boltzmann analytical gradients for molecular modeling calculations. *J Phys Chem B*. 1999;103:3057–61. <https://doi.org/10.1021/jp982513m>
119. Otani M, Sugino O. First-principles calculations of charged surfaces and interfaces: a plane-wave nonrepeated slab approach. *Phys Rev B*. 2006;73:115407. <https://doi.org/10.1103/physrevb.73.115407>
120. Jinnouchi R, Anderson AB. Electronic structure calculations of liquid-solid interfaces: combination of density functional theory and modified Poisson–Boltzmann theory. *Phys Rev B*. 2008;77:245417. <https://doi.org/10.1103/physrevb.77.245417>
121. Borukhov I, Andelman D, Orland H. Steric effects in electrolytes: a modified Poisson–Boltzmann equation. *Phys Rev Lett*. 1997;79:435–8. <https://doi.org/10.1103/physrevlett.79.435>
122. Nattino F, Truscott M, Marzari N, Andreussi O. Continuum models of the electrochemical diffuse layer in electronic-structure calculations. *J Chem Phys*. 2019;150:041722. <https://doi.org/10.1063/1.5054588>
123. Wang X, Liu K, Wu J. Demystifying the stern layer at a metal–electrolyte interface: local dielectric constant, specific ion adsorption, and partial charge transfer. *J Chem Phys*. 2021;154:124701.
124. Heenen HH, Gauthier JA, Kristoffersen HH, Ludwig T, Chan K. Solvation at metal/water interfaces: an ab initio molecular dynamics benchmark of common computational approaches. *J Chem Phys*. 2020;152:144703. <https://doi.org/10.1063/1.5144912>
125. Le J, Iannuzzi M, Cuesta A, Cheng J. Determining potentials of zero charge of metal electrodes versus the standard hydrogen electrode from density-functional-theory-based molecular dynamics. *Phys Rev Lett*. 2017;119:016801. <https://doi.org/10.1103/physrevlett.119.016801>
126. Golze D, Iannuzzi M, Nguyen M-T, Passerone D, Hutter J. Simulation of adsorption processes at metallic interfaces: an image charge augmented QM/MM approach. *J Chem Theory Comput*. 2013;9:5086–97. <https://doi.org/10.1021/ct400698y>
127. Hörmann NG, Guo Z, Ambrosio F, Andreussi O, Pasquarello A, Marzari N. Absolute band alignment at semiconductor-water interfaces using explicit and implicit descriptions for liquid water. *Npj Comput Mater*. 2019;5:100. <https://doi.org/10.1038/s41524-019-0238-4>
128. Lozovoi AY, Alavi A, Kohanoff J, Lynden-Bell RM. Ab initio simulation of charged slabs at constant chemical potential. *J Chem Phys*. 2001;115:1661–9. <https://doi.org/10.1063/1.1379327>
129. Tavernelli I, Vuilleumier R, Sprik M. Ab initio molecular dynamics for molecules with variable numbers of electrons. *Phys Rev Lett*. 2002;88:213002. <https://doi.org/10.1103/physrevlett.88.213002>
130. Bonnet N, Morishita T, Sugino O, Otani M. First-principles molecular dynamics at a constant electrode potential. *Phys Rev Lett*. 2012;109:266101. <https://doi.org/10.1103/physrevlett.109.266101>
131. Sundararaman R, Goddard WA, Arias TA. Grand canonical electronic density-functional theory: algorithms and applications to electrochemistry. *J Chem Phys*. 2017;146:114104. <https://doi.org/10.1063/1.4978411>
132. Hörmann NG, Andreussi O, Marzari N. Grand canonical simulations of electrochemical interfaces in implicit solvation models. *J Chem Phys*. 2019;150:041730. <https://doi.org/10.1063/1.5054580>
133. Bouzid A, Pasquarello A. Atomic-scale simulation of electrochemical processes at electrode/water interfaces under referenced bias potential. *J Phys Chem Lett*. 2018;9:1880–4. <https://doi.org/10.1021/acs.jpclett.8b00573>
134. Surendralal S, Todorova M, Finnis MW, Neugebauer J. First-principles approach to model electrochemical reactions: understanding the fundamental mechanisms behind mg corrosion. *Phys Rev Lett*. 2018;120:246801. <https://doi.org/10.1103/physrevlett.120.246801>
135. Dufils T, Jeanmairet G, Rotenberg B, Sprik M, Salanne M. Simulating electrochemical systems by combining the finite field method with a constant potential electrode. *Phys Rev Lett*. 2019;123:195501. <https://doi.org/10.1103/physrevlett.123.195501>
136. Goodpaster JD, Bell AT, Head-Gordon M. Identification of possible pathways for C–C bond formation during electrochemical reduction of CO<sub>2</sub>: new theoretical insights from an improved electrochemical model. *J Phys Chem Lett*. 2016;7:1471–7. <https://doi.org/10.1021/acs.jpclett.6b00358>

137. Rossmeisl J, Skúlason E, Björketun ME, Tripkovic V, Nørskov JK. Modeling the electrified solid–liquid interface. *Chem Phys Lett.* 2008;466:68–71. <https://doi.org/10.1016/j.cplett.2008.10.024>
138. Fang Y-H, Wei G-F, Liu Z-P. Theoretical modeling of electrode/electrolyte interface from first-principles periodic continuum solvation method. *Catal Today.* 2013;202:98–104. <https://doi.org/10.1016/j.cattod.2012.04.055>
139. Taylor CD, Wasileski SA, Filhol J-S, Neurock M. First principles reaction modeling of the electrochemical interface: consideration and calculation of a tunable surface potential from atomic and electronic structure. *Phys Rev B.* 2006;73:165402. <https://doi.org/10.1103/physrevb.73.165402>
140. Duan S, Xu X, Tian Z-Q, Luo Y. Hybrid molecular dynamics and first-principles study on the work function of a Pt(111) electrode immersed in aqueous solution at room temperature. *Phys Rev B.* 2012;86:045450. <https://doi.org/10.1103/physrevb.86.045450>
141. Hansen MH, Rossmeisl J. pH in grand canonical statistics of an electrochemical Interface. *J Phys Chem C.* 2016;120:29135–43.
142. Zhang C, Sayer T, Hutter J, Sprik M. Modelling electrochemical systems with finite field molecular dynamics. *J Phys Energy.* 2020;2: 032005. <https://doi.org/10.1088/2515-7655/ab9d8c>
143. Zhang C, Sprik M. Finite field methods for the supercell modeling of charged insulator/electrolyte interfaces. *Phys Rev B.* 2016;94: 245309. <https://doi.org/10.1103/physrevb.94.245309>
144. Sayer T, Zhang C, Sprik M. Charge compensation at the interface between the polar NaCl(111) surface and a NaCl aqueous solution. *J Chem Phys.* 2017;147:104702. <https://doi.org/10.1063/1.4987019>
145. Zhang C. Note: on the dielectric constant of nanoconfined water. *J Chem Phys.* 2018;148:156101. <https://doi.org/10.1063/1.5025150>
146. Sayer T, Sprik M, Zhang C. Finite electric displacement simulations of polar ionic solid-electrolyte interfaces: application to NaCl (111)/aqueous NaCl solution. *J Chem Phys.* 2019;150:041716. <https://doi.org/10.1063/1.5054843>
147. Zhang C, Hutter J, Sprik M. Computing the Kirkwood g-factor by combining constant Maxwell electric field and electric displacement simulations: application to the dielectric constant of liquid water. *J Phys Chem Lett.* 2016;7:2696–701. <https://doi.org/10.1021/acs.jpclett.6b01127>
148. Zhang C, Hutter J, Sprik M. Coupling of surface chemistry and electric double layer at TiO<sub>2</sub> electrochemical interfaces. *J Phys Chem Lett.* 2019;10:3871–6. <https://doi.org/10.1021/acs.jpclett.9b01355>
149. Stengel M, Spaldin NA, Vanderbilt D. Electric displacement as the fundamental variable in electronic-structure calculations. *Nat Phys.* 2009;5:304–8. <https://doi.org/10.1038/nphys1185>
150. Behler J, Parrinello M. Generalized neural-network representation of high-dimensional potential-energy surfaces. *Phys Rev Lett.* 2007; 98:146401. <https://doi.org/10.1103/physrevlett.98.146401>
151. Bartók AP, Payne MC, Kondor R, Csányi G. Gaussian approximation potentials: the accuracy of quantum mechanics, without the electrons. *Phys Rev Lett.* 2010;104:136403. <https://doi.org/10.1103/physrevlett.104.136403>
152. Zhang L, Wang H, Weinan E. Adaptive coupling of a deep neural network potential to a classical force field. *J Chem Phys.* 2018;149: 154107. <https://doi.org/10.1063/1.5042714>
153. Zhang L, Han J, Wang H, Car R, Weinan E. DeePCG: constructing coarse-grained models via deep neural networks. *J Chem Phys.* 2018;149:034101. <https://doi.org/10.1063/1.5027645>
154. Zhang Y, Wang H, Chen W, Zeng J, Zhang L, Wang H, et al. DP-GEN: a concurrent learning platform for the generation of reliable deep learning based potential energy models. *Comput Phys Commun.* 2020;253:107206. <https://doi.org/10.1016/j.cpc.2020.107206>
155. Grisafi A, Ceriotti M. Incorporating long-range physics in atomic-scale machine learning. *J Chem Phys.* 2019;151:204105. <https://doi.org/10.1063/1.5128375>

**How to cite this article:** Yang X-H, Zhuang Y-B, Zhu J-X, Le J-B, Cheng J. Recent progress on multiscale modeling of electrochemistry. *WIREs Comput Mol Sci.* 2021;e1559. <https://doi.org/10.1002/wcms.1559>